Thermodynamic and spectral properties of compressed Ce calculated by the merger of the local density approximation and dynamical mean field theory

A. K. McMahan,[1] K. Held,[2] and R. T. Scalettar[3]
[1] *Lawrence Livermore National Laboratory, University of California, Livermore, CA 94550*
[2] *Max-Planck-Institut für Festkörperforschung, D-70569 Stuttgart, Germany*
[3] *Physics Department, University of California, Davis, CA 95616*
(Dated: February 1, 2008)

We have calculated thermodynamic and spectral properties of Ce metal over a wide range of volume and temperature, including the effects of $4f$ electron correlations, by the merger of the local density approximation and dynamical mean field theory (DMFT). The DMFT equations are solved using the quantum Monte Carlo technique supplemented by the more approximate Hubbard I and Hartree Fock methods. At large volume we find Hubbard split spectra, the associated local moment, and an entropy consistent with degeneracy in the moment direction. On compression through the volume range of the observed γ-α transition, an Abrikosov-Suhl resonance begins to grow rapidly in the $4f$ spectra at the Fermi level, a corresponding peak develops in the specific heat, and the entropy drops rapidly in the presence of a persistent, although somewhat reduced local moment. Our parameter-free spectra agree well with experiment at the α- and γ-Ce volumes, and a region of negative curvature in the correlation energy leads to a shallowness in the low-temperature total energy over this volume range which is consistent with the γ-α transition. As measured by the double occupancy, we find a noticeable decrease in correlation on compression across the transition; however, even at the smallest volumes considered, Ce remains strongly correlated with residual Hubbard bands to either side of a dominant Fermi-level structure. These characteristics are discussed in light of current theories for the volume collapse transition in Ce.

PACS numbers: 71.27.+a, 71.20.Eh, 75.20.Hr

I. INTRODUCTION

A number of rare earth metals undergo pressure induced first order phase transitions with unusually large volume changes of 9–15% (for reviews see Refs. 1,2,3). Of these transitions the isostructural γ-α transition in Ce has received the most attention.[4] It was discovered first, has the largest volume change (15% at room temperature), and may also be accessed entirely at ambient pressure (or in vacuum) by changing the temperature, thus, for example, allowing thorough spectroscopic investigation of both phases. The results of such photoemission and Bremsstrahlung studies[5] show a dramatic transfer of spectral weight to the Fermi energy and the development of a large peak with its center of gravity slightly above the Fermi energy when going from the γ- to the α-Ce phase. Similarly, the optical conductivity is higher in the α phase where the frequency dependent scattering rate is characteristic for a Fermi liquid behavior with an effective mass of about $20\,m_e$.[6] Also the magnetic susceptibility and its temperature dependence change from a Curie-Weiss like behavior in the γ phase to a Pauli paramagnetic behavior in the α phase.[4] Despite these dramatic differences, the number of $4f$ electrons does not change significantly and is close to one across the γ-α phase transition line which ends in a critical point at $T = 600 \pm 50\,\mathrm{K}$,[4] above which the γ- and α-Ce phases become indistinguishable.

Notwithstanding the considerable attention, there remains continued disagreement about the nature of the transition and the α phase. In general, it is believed that the transition is driven by changes in the $4f$ electron correlations, though some alternative theories have been proposed. Two recent examples of the latter assume some kind of symmetry breaking in the α phase: Eliashberg and Capellmann[7] argue that α-Ce has a symmetry broken distorted structure mainly based on the observation that the α phase shows large changes of the compressibility;[8] Nikolaev and Michel[9] propose (hidden) quadrupolar ordering. In these theories a critical endpoint is impossible because of the symmetry breaking, and there must be, at least, a second order phase transition line above $T \sim 600\,\mathrm{K}$, which disagrees with the common interpretation of the experiment.[4]

The first theory of electronic origin to describe the γ-α transition was the promotional model[10] which assumed a change in the electronic configuration from $4f^1(spd)^3$ to $4f^0(spd)^4$. However, it was soon ruled out by experiment which did not reveal any major change in the number of $4f$ electrons. Also band structure calculations found about one $4f$ electron per Ce atom in the α phase, leading Johansson to propose a Mott transition (MT) scenario.[11] Similar to the MT of the Hubbard model, the $4f$ electrons are considered to be localized in the γ phase and to be itinerant in the α phase, with this reduction in the degree of $4f$-electron correlation being caused by the decrease in the ratio of Coulomb interaction to kinetic energy under pressure. In a subsequent analysis based on these ideas, Johansson *et al.*[12] employed a standard local density approximation (LDA) calculation for the *spdf* electrons in the α phase, while treating the $4f$ electrons as localized $4f^1$ moments decoupled from LDA *spd* bands in the γ phase. Evidence for the MT scenario to be correct is taken from the considerable suc-

cess of LDA calculations and their generalized gradient improvements for the structural and volume dependence of the total energy of α-Ce-like phases.[13,14] Additional support appears to come from orbitally polarized[15,16,17] and self-interaction corrected[17,18,19] LDA modifications which obtain transitions in Ce and Pr at about the right pressures. Also LDA+U calculations have been reported for one or both Ce phases.[20,21]

This MT model appears in conflict with the Kondo volume collapse (KVC) scenario of Allen and Martin[22] and Lavagna *et al.*[23] which is based on the Anderson impurity model. Both pictures agree that, at the experimental temperatures, the larger volume γ phase is strongly correlated (localized), has Hubbard split $4f$ spectra, and exhibits a Hund's rule $4f^1$ moment as reflected in the observed Curie-Weiss magnetic susceptibility. But, while the MT scenario then envisages a rather abrupt transition on compression to a weakly correlated (itinerant) α phase, in which the Hubbard split bands have coalesced together near the Fermi level and the $4f^1$ moments are lost, the KVC picture assumes continued strong correlation in the α phase with Kondo screening of the $4f$ moments by the valence electrons. The signature of this Kondo screening is a peak in the $4f$ spectra at the Fermi level, the Abrikosov-Suhl resonance, which lies between the remaining Hubbard-split spectral weight characteristic of the local moment.[5] Assuming a rapid volume dependence of the Kondo temperature, there is Kondo screening and an Abrikosov-Suhl resonance in the α phase but not in the γ phase since the Kondo temperature of the α phase is above and that of the γ phase below the typical experimental temperatures. The strong volume dependence of the Kondo temperature leads to a region of negative curvature in the free energy and, thence, a first order transition as dictated by the common (Maxwell) tangent construction,[22,23] similar to a vapor-liquid transition. While the KVC model provides a genuine many-body calculation for Ce, it nevertheless incorporates only two bands, which has prompted previous attempts at introducing more orbital realism from LDA.[24,25]

On the basis of the underlying Hubbard and periodic Anderson models, it has been argued recently that the MT and KVC scenarios are rather similar when the important many-body effects are taken into account.[26] That is, the behavior of the local moment at the MT of the Hubbard model is not so abrupt, nor is the appearance of a three peak structure in the density of states unique to the periodic Anderson model. This fact can be obscured by the use of static mean-field approximations (including LDA and its modifications) especially when describing the α phase.

A new approach to describe Ce including both orbital realism and electronic correlation effects is now available with the recent merger[27,28,29] of LDA and dynamical mean field theory (DMFT).[30,31] This approach has been employed by Zölfl *et al.*[32] who used the non-crossing approximation (NCA) to solve the DMFT equations in order to calculate the spectra, Kondo temperatures, and susceptibilities for α- and γ-Ce. Independently, we treated the DMFT equations with the more rigorous Quantum Monte Carlo[33] (QMC) simulations and reported, as first results of the present effort, evidence for a Ce volume collapse in the total LDA+DMFT energy which coincides with dramatic changes in the $4f$ spectrum.[34] A similar transition was also described earlier in LDA+DMFT calculations for Pu.[35] In all three cases, the f spectra showed Abrikosov-Suhl resonances lying in between residual Hubbard splitting for the smaller-volume, less-correlated α phases, in contrast to the LDA results mentioned above which only obtain the Fermi-level structure. Related behavior is also observed for the Mott transition in V_2O_3, which was studied recently by LDA+DMFT.[36]

In the present work we extend Ref. 34 to lower temperatures, complement it with Hubbard-I calculations,[28,37] and calculate the volume-dependence of additional physical quantities including the entropy, specific heat, total spectrum, orbital occupation, and the magnetic moment. In Section II, the LDA+DMFT technique is briefly described along with the Hubbard-I approximation and a new and faster implementation of the QMC treatment which is subsequently validated against established approaches. In Section III, thermodynamic results, i.e., the energy, specific heat, entropy, and free energy, are presented over a wide range of volume and temperature and the signatures for the α-γ transition are discussed. We present the volume- and temperature-dependence of the $4f$- and the valence *spd*-spectrum and compare to experiment in Section IV. The $4f$ occupation, local magnetic moment, and related quantities are given in Section V. Finally, the results of this paper are summarized and discussed in Section VI.

II. THEORETICAL METHODS

The results in this paper have been obtained by the LDA+DMFT method, that is by the merger of the local density approximation (LDA) and dynamical mean-field theory (DMFT) which was recently introduced by Anisimov *et al.*[27] and Lichtenstein and Katsnelson[28] (for an introduction see Ref. 29). The starting point of this method is a conventional LDA band structure calculation. Since electronic correlations are only treated at a mean field level within LDA, the most important term for electronic correlations, i.e., the local Coulomb interaction, is added explicitly. This defines a multi-band many-body problem which is solved by DMFT. To solve the DMFT equations, we employ two different implementations of the quantum Monte Carlo (QMC) technique as well as the Hubbard-I[28,37] (H-I) approximation. This section describes the relevant computational details of our calculations.

A. LDA+DMFT approach

Scalar-relativistic, linear muffin-tin orbital LDA calculations[38,39] were performed for face centered cubic (fcc) Ce over a grid of volumes as described elsewhere.[3] The associated $(6s, 6p, 5d, 4f)$ one-electron Hamiltonians define 16×16 matrices $H^0_{\rm LDA}$, after shifting the $4f$ site energies to avoid double counting the Coulomb interaction U_f between $4f$ electrons. The latter is explicitly taken into account in the full second-quantized Hamiltonian for the electrons,

$$H = \sum_{\mathbf{k},lm,l'm',\sigma} (H^0_{\rm LDA}(\mathbf{k}))_{lm,l'm'}\, \hat{c}^\dagger_{\mathbf{k}\,lm\sigma}\hat{c}_{\mathbf{k}\,l'm'\sigma} + \frac{1}{2}\,U_f \sum_{\mathbf{i},m\sigma,m'\sigma'}{}' \hat{n}_{\mathbf{i}fm\sigma}\,\hat{n}_{\mathbf{i}fm'\sigma'}. \quad (1)$$

Here, $\mathbf{k}$ are Brillouin zone vectors, $\mathbf{i}$ are lattice sites, lm denote the angular momentum, σ is the spin quantum number, $\hat{n}_{\mathbf{i}fm\sigma} \equiv \hat{c}^\dagger_{\mathbf{i}fm\sigma}\hat{c}_{\mathbf{i}fm\sigma}$, and the prime signifies $m\sigma \neq m'\sigma'$. The many-body Hamiltonian Eq. (1) has *no* free parameters since we employed constrained-occupation LDA calculations to determine U_f and the $4f$ site energy shift for all volumes considered (see Fig. 5 of Ref. 3 for the values). We did not take into account the spin-orbit interaction which has a rather small impact on LDA results for Ce, and also neglected the intra-atomic exchange interaction which has only an effect if there are more than one $4f$-electrons on a Ce atom.

The DMFT maps the lattice problem Eq. (1) onto the self-consistent solution of the Dyson equation

$$G_{\mathbf{k}}(i\omega) = \left[\, i\omega I + \mu I - H^0_{\rm LDA}(\mathbf{k}) - \Sigma(i\omega) I_f \right]^{-1}, \quad (2)$$

and a seven-orbital (auxiliary) impurity problem defined by the bath Green function

$$\mathcal{G}(i\omega)^{-1} = \left(\frac{1}{7N} \sum_{\mathbf{k}} Tr\{G_{\mathbf{k}}(i\omega) I_f\} \right)^{-1} + \Sigma(i\omega). \quad (3)$$

Here I is the unit matrix, $I_f \equiv [\delta_{lf}\delta_{l'f}\delta_{mm'}]$ projects onto the seven f-orbitals, μ is the chemical potential, Tr denotes the trace over the orbital matrix, and N is the number of $\mathbf{k}$ points ($N = 2048$ for $T \leq 0.4\,$eV and $N = 256$ for $T > 0.4\,$eV). Within the LDA, there is a minor crystal-field splitting of the seven $4f$ orbitals. However, in Eq. (3) we average over the seven $4f$ orbitals, i.e., we treat them as degenerate in the auxiliary impurity problem. Consequently the DMFT self-energy is diagonal $\Sigma(i\omega)I_f$, at least in the paramagnetic phase studied. The impurity problem is solved with one of the methods described in the following two sections and generates a self-energy $\Sigma(i\omega)$. This self-energy gives a new Green function in Eq. (2) and thus a new impurity problem and so on, iterating to self-consistency (for more details see Refs. 31 and 29). In this self-consistency cycle, the chemical potential μ of Eq. (2) is adjusted so that the total number electrons described by Eq. (1) is $n_f + n_v = 4$ per Ce site. Here, the number of $4f$ electrons n_f, and similarly the number n_v of valence (i.e., *spd*) electrons, may be obtained from the lattice Green function

$$n_f = \frac{T}{N} \sum_{n\mathbf{k}\sigma} {\rm Tr}\,[G_{\mathbf{k}}(i\omega_n) I_f]\, e^{i\omega_n 0^+}\,, \quad (4)$$

where T is the temperature and $\omega_n = (2n+1)\pi T$ are the Matsubara frequencies. To obtain the physically relevant Green function $G(\omega)$, we employ the maximum entropy method[40] for the analytic continuation to real frequencies ω.

In principle the LDA and DMFT parts of the calculation should be mutually self-consistent, with DMFT changes in orbital occupations (especially n_f) feeding back into a new $H^0_{\rm LDA}(\mathbf{k})$ and U_f, as argued by Savrasov and coworkers.[35] Certainly the constrained occupation calculations used to fix U_f and the $4f$ site energy in $H^0_{\rm LDA}(\mathbf{k})$ should not be impacted, as they are intended to be valid over the range $0 < n_f < 2$. These calculations provide what are in effect the screened Coulomb energies for 0, 1, and 2 f electrons per site, which covers this range according to what fraction of the sites are at one or another of the various occupations.[3] However, differences between the DMFT n_f and the LDA n_f could, if the former were fed back into the LDA, change the position of $4f$ level slightly, and with that the extension of the $4f$ wavefunction, and thus the f-valence hybridization. It is simply not known at this point if such effects are important, although we note that DMFT(QMC) and LDA-like (see Sec. II D) solutions of Eq. (1) generally yield values of n_f within 10% of one another. The additional cost on top of the already very expensive LDA+DMFT(QMC) method also makes such additional self-consistency impractical in the present case.

B. Hubbard-I approximation

In the large-volume limit where intersite hybridization vanishes, the auxiliary impurity problem is simply the isolated atom, i.e., $\mathcal{G}(i\omega) = 1/(i\omega + \mu - \varepsilon_f)$ where ε_f is the $4f$ site energy. In this limit the exact self-energy is known and may, at finite volumes, be used as the Hubbard-I (H-I) approximation[28,37]:

$$\Sigma^{\rm at}(i\omega) \;=\; i\omega + \mu_{\rm at} - [G^{\rm at}(i\omega)]^{-1}, \quad (5)$$

$$G^{\rm at}(i\omega) \;=\; \sum_{j=1}^{14} \frac{w_j(\mu_{\rm at}, T)}{i\omega + \mu_{\rm at} - (j-1)U_f}, \quad (6)$$

$$n_f^{\rm at} \;=\; 14T \sum_n G^{\rm at}(i\omega_n) e^{i\omega_n 0^+}, \quad (7)$$

where ε_f has been absorbed into $\mu_{\rm at}$, which is set at each iteration in such a way that $n_f^{\rm at}$ of Eq. (7) equals the current n_f of Eq. (4). The positive weights w_j for

transitions between $j-1$ and j electrons are given by

$$w_j \;=\; [jv_j + (15-j)v_{j-1}]/(14\sum_{l=0}^{14} v_l)\,, \qquad (8)$$

where v_j are Boltzmann weights for having j electrons on the atom

$$v_j \;=\; \frac{14!}{j!(14-j)!}\exp\left[-\{\tfrac{1}{2}j(j-1)U_f - j\mu_{\rm at}\}/T\right]. \qquad (9)$$

Our DMFT(H-I) procedure is in fact also correct at *all* volumes in the high-temperature limit. Noting that the w_j's sum to unity, one can see that

$$\Sigma^{\rm at}(\infty) = \frac{13}{14}U_f\sum_{j=0}^{14} jv_j/\sum_{j=0}^{14} v_j = \frac{13}{14}n_f U_f\,, \qquad (10)$$

since we always choose $\mu_{\rm at}$ so that $n_f^{\rm at}=n_f$. This is the paramagnetic Hartree-Fock value, which is also the correct high-temperature limit since the $\omega_n \propto T$, and only the high-frequency tail of the self-energy is of importance.

C. QMC simulations

Our main approach to solve the DMFT impurity problem is the numerical QMC technique. We use two implementations which differ mainly by the Fourier transformation between the Matsubara frequency representation employed in the Dyson equation Eq. (2) and the imaginary time representation employed for the QMC simulation of the impurity problem Eq. (3). Within QMC, the imaginary time interval $[0,\beta]$ ($\beta = 1/T$) is discretized into Λ Trotter slices of size $\Delta\tau = \beta/\Lambda$. Since there are 91 Ising fields *per* time slice, the number of time slices which are computationally manageable in the QMC is seriously restricted. Thus, if one employs a discrete Fourier transformation between $\mathcal{G}(i\omega_n)$ at a finite number of Λ Matsubara frequencies and $\mathcal{G}(\tau_l), \tau_l = 1\Delta\tau, \ldots, \Lambda\Delta\tau$, the resulting Green function oscillates considerably around the correct $\mathcal{G}(\tau)$. To overcome this shortcoming, Ulmke and coworkers[41] suggested using a smoothing procedure which replaces $\mathcal{G}(i\omega_n) \rightarrow \tilde{\mathcal{G}}(i\omega_n)$, after calculating the auxiliary $\mathcal{G}(i\omega_n)$ via Eq. (3), where

$$\tilde{\mathcal{G}}(i\omega_n) \equiv \frac{\Delta\tau}{1-\exp[-\Delta\tau/\mathcal{G}(i\omega_n)]}\,. \qquad (11)$$

It is $\tilde{\mathcal{G}}(i\omega_n)$ that is Fourier transformed to imaginary time $\mathcal{G}(\tau_l)$, and once the QMC simulations of the Anderson impurity problem have yielded the output $G(\tau_l)$, the process is reversed: The Fourier transform of $G(\tau_l)$, $\tilde{G}(i\omega_n)$, yields $G(i\omega_n)$ from the inverse of Eq. 11. The new self-energy is then $\Sigma(i\omega_n) = \mathcal{G}(i\omega_n)^{-1} - G(i\omega_n)^{-1}$.

This approach generates smooth Green functions $G(\tau_l)$ and reproduces the correct $\Delta\tau \rightarrow 0$ limit. We use it in one implementation of the QMC algorithm, referred to as QMC_1 in the following. Other approaches employed in the literature are to fit splines to $G(\tau_l)$ and, thus, to use more support points than Λ to do the Fourier transformation[31] or to extend the Matsubara frequency sums by employing the iterated perturbation theory result at high frequencies.[33] Most results of our paper were obtained by yet another QMC implementation (QMC_2) which uses a different way to Fourier transform and which seems to be less sensitive to statistical noise. As this modification is new, it is described in some detail in Section II C 1 and validated in Section II C 2.

1. Modified QMC implementation

In the implementation QMC_2, we use a constrained fit

$$G(\tau) = \sum_i w_i f_i(\tau). \qquad (12)$$

to the output QMC impurity Green function $G(\tau_l)$, in order to accomplish the Fourier transform to $G(i\omega_n)$ for $n = -\frac{1}{2}N_\omega, \ldots, \frac{1}{2}N_\omega - 1$ with $N_\omega > \Lambda$. The basis functions are $f_i(\tau) = -e^{-\varepsilon_i\tau}/(e^{-\beta\varepsilon_i}+1)$ and have Fourier transforms $f_i(i\omega) = 1/(i\omega-\varepsilon_i)$. At real frequencies, Eq. (12) corresponds to a set of δ-functions with different spectral weights w_i, and is capable in the limit of an infinite set of basis functions of reproducing any given spectrum. In contrast to a spline-fit where every fit-coefficient is determined by the local behavior in an imaginary time interval, in our approach every fit-coefficient is determined by the local behavior in frequency space.

The constraints to the fit Eq. (12) are $w_i \geq 0$, $G(0^+)$ is precisely the QMC value, $G(0^+)+G(\beta^-) = -1$, and $\frac{d}{d\tau}G(0^+)+\frac{d}{d\tau}G(\beta^-) = \mathrm{g}_2$, where $\beta^- \equiv \beta - 0^+$ and g_m is the $(i\omega)^{-m}$ high-frequency moment of $G(i\omega)$. For the last constraint, g_2 is obtained from the relation $G^{-1}(i\omega) = \mathcal{G}^{-1}(i\omega) - \Sigma(i\omega)$ which implies $\mathrm{g}_2 = g_2 + \mathrm{s}_0$, where these are the indicated moments of $G(i\omega)$, $\mathcal{G}(i\omega)$, and $\Sigma(i\omega)$, respectively. Here, g_2 is known as $\mathcal{G}$ is input to the QMC, and we take $s_0 = \Sigma(i\omega=\infty) = (13/14)n_f U_f$ with $n_f = 14[1+G(\tau=0^+)]$ for the present paramagnetic case.[42]

Typically we use grids of $\Lambda/4$ equally spaced ε_i, and optimize the agreement with the QMC data as a function of the centroid and width of these grids, in each case systematically eliminating basis functions for a given grid which would otherwise yield negative w_i. Because the QMC expense increases as Λ^3, we are forced to execute fewer Monte Carlo sweeps for the largest Λ's, and the statistics become less good than for smaller Λ's. However, the constraint $w_i \geq 0$ still seems to provide a sensible interpolation through the statistical noise, although this has the consequence that the number of surviving positive w_i increases more slowly than Λ. Nonetheless, we see a systematic evolution as a function of Λ and extrapolations $\Lambda \rightarrow \infty$ agree with large-volume and high-temperature limits (Hubbard-I) and the QMC_1 (see Section II C 2). Note that while we find the fit Eq. (12) to

be very useful for functional behavior along the imaginary time and frequency axes, and for integral quantities such as n_f and the total energy, it is not useful in practice for directly obtaining real frequency behavior in the presence of typical QMC statistical uncertainties. The maximum entropy method is far superior here as it folds these uncertainties into calculation of the spectra.[40]

In order to accelerate the convergence of our DMFT(QMC$_2$) method we carry out cheap iterations on the constant part of the self-energy in between each expensive QMC iteration. That is, we subtract a constant Hartree-Fock contribution[42] from the QMC self energy: $\Delta\Sigma(i\omega) = \Sigma^{\rm QMC}(i\omega) - (13/14)n_f^{\rm QMC}U_f$ where $n_f^{\rm QMC} = 14[1+G(\tau=0^+)]$. Following every QMC cycle, then, one has $\Sigma(i\omega) = (13/14)n_fU_f + \Delta\Sigma(i\omega)$ in Eq. (2) which is iterated to self-consistency with n_f from Eq. (4), while keeping $\Delta\Sigma$ fixed. The resultant values of n_f and $n_f^{\rm QMC}$ agree within statistical uncertainties. These uncertainties can be significantly smaller for n_f than for $n_f^{\rm QMC}$ at the smallest volumes.

We find $G(\tau)$ to converge quickly as a function of QMC$_2$ iteration for all τ at small volume, and for τ close to 0 and β at large volume. For intermediate τ at large volume and low temperature, however, where $G(\tau)$ is generally quite small, convergence appears to result from the average of frequent small values of $G(\tau)$ with occasional large values as the Ising configurations are sampled, with the large-volume atomic limit approached by the latter becoming statistically unimportant.

In order to improve the statistics given this behavior, we have chosen to include sweeps from all previous QMC iterations (excluding warm up sweeps) along with the new sweeps in $G_i^{\rm new}(\tau_l)$ in arriving at the QMC$_2$ result for iteration i: $G_i(\tau_l) = [G_i^{\rm new}(\tau_l) + (i-1)G_{i-1}(\tau_l)]/i$. Note that the warm-up sweeps themselves are already started with a reasonable self-energy, such as a converged DMFT(H-I) result or a DMFT(QMC$_2$) result for another Λ. We have tested this treatment at both small and large volumes by starting anew at $i=1$ from the converged DMFT(QMC$_2$) self-energy, and have found agreement with the previous results to within statistical uncertainties.

We used 10,000 sweeps per QMC iteration for $\Lambda=80$, decreasing systematically to 1,000 for $\Lambda=256$, and carried out from 20 to over 100 QMC iterations for each T, V point. At small V even at $T=0.054$ eV we found the DMFT(QMC$_2$) energy to settle down generally after a few QMC$_2$ iterations to maximal excursions of about ±0.02 eV (±0.05 eV) for $\Lambda=80$ (256), with the root-mean-square uncertainties much smaller. Such benign behavior extends to increasingly large volumes at higher T, where these DMFT(QMC$_2$) results begin to agree closely with DMFT(H-I). At low temperature, the scatter in our measurements as a function of iteration grows as volume is increased, especially in the transition region and beyond; however, the Trotter corrections also diminish here so there is less need for larger Λ.

Finally, we turn to the issue of performing the Fourier transform from imaginary time to Matsubara frequencies. The virtue of the fit Eq. (12) is that it decouples Λ and N_ω allowing manageable QMC costs (smaller Λ) and yet accurate kinetic energies (larger N_ω). Most of our DMFT(QMC$_2$) calculations took $N_\omega=256$ for $T\geq0.054$ eV and $N_\omega=512$ for $T=0.027$ eV. In the course of this work we realized that there is a volume dependence to the error in the kinetic energy from the Matsubara cutoff, and while the $N_\omega=256$ choice at $T=0.054$ eV leads to a small 0.04 eV error in the vicinity of the transition, it becomes more significant, 0.11 eV, at the smallest volumes considered. Since our DMFT(H-I) and DMFT(QMC$_2$) codes have identical kinetic energy treatment, we used the former to correct the present DMFT(QMC$_2$) results to effective values of N_ω four times those just noted, which should give better than 0.01 eV accuracy at all volumes. We verified this by selected DMFT(QMC$_2$) tests with the larger N_ω. Note that this kinetic energy treatment includes (and the cited errors reflect) an approximate evaluation of the full infinite Matsubara sum. Specifically, we approximate the high-frequency behavior of a quantity $F(i\omega)$ by $F_0(i\omega)=w_1/(i\omega-\varepsilon_1)+w_2/(i\omega-\varepsilon_2)$, with parameters chosen to reproduce its $1/(i\omega)^m$ moments for $m=1$–4. Then we approximate the infinite Matsubara sum on $F(i\omega)$ by the analytic result for the infinite sum over F_0 plus the finite sum over the difference $F-F_0$.

2. Validation

Here we validate the new faster QMC$_2$ algorithm of Sec. II C 1, used for much of the low-temperature thermodynamic results in this paper, against QMC$_1$ which employs the Ulmke-smoothing. Such validation involves extrapolation to the limits $N_\omega, \Lambda \to \infty$, where the QMC$_1$ approach should provide exact results. Errors which vanish in these limits include those arising from truncation of Matsubara sums (finite N_ω), and from the Trotter approximation (finite Λ).

Figure 1 compares the kinetic DMFT energy (see Section II D for details of its calculation) obtained by QMC$_2$ and QMC$_1$ as a function of $\Delta\tau=\beta/\Lambda$, at a temperature $T=0.54$ eV and atomic volume $V=16.8$ Å^3. (Note that the $\Delta\tau$ dependence is largest at small volumes, as we shall discuss further.) The line with open circles shows the QMC$_1$ results with Matsubara sums truncated after $N_\omega=\Lambda$ frequencies under the application of Ulmke's smoothing procedure Eq. (11). Those with squares and open triangles show the results when these sums are extended to $N_\omega=\infty$ using the Hartree-Fock (HF) Green function at high Matsubara frequencies; that is, using Eq. (2) with $\Sigma\to\Sigma_{\rm HF}=(13/14)n_fU_f$ for $\pm\omega=\Lambda\pi T,\ldots,\infty$.[43] In the first case (squares) the current chemical potential μ and n_f were used to define $\Sigma_{\rm HF}$. In the second case (open triangles) the whole procedure was made self-consistent: From n_f, we calculate

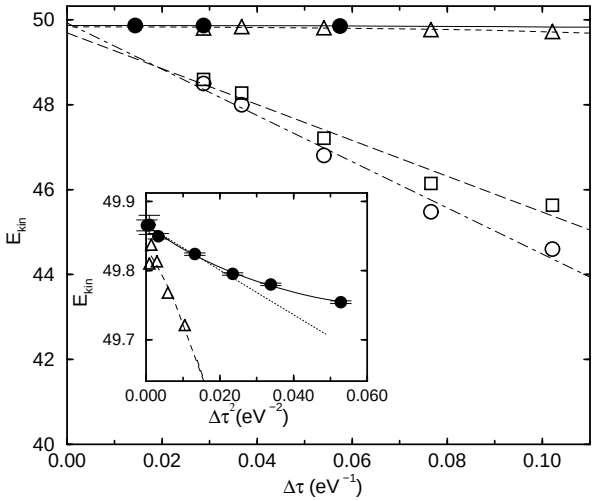

FIG. 1: Extrapolation $\Delta\tau \to 0$ of the kinetic energy at $T = 0.54\,\text{eV}$ and $V = 16.8\,\text{Å}^3$, using the QMC_2 (filled circles) and the QMC_1 algorithm (open circles, squares, and triangles; differences are due to whether and how Hartree-Fock results for the high-frequency tails of self-energy are included, see text). The lines show the extrapolations through the QMC data yielding $E_{\text{kin}}(\Delta\tau = 0) = 49.888 \pm 0.003$ eV (filled circles) and $49.853 \pm 0.022\,\text{eV}$ (open triangles), both with a mixed quadratic and cubic fit; and 49.944 ± 0.271 eV (open circles) and $49.713 \pm 0.305\,\text{eV}$ (open squares), both with a linear fit. The results agree within twice the above standard deviation and, thus, validate, the QMC_2 algorithm. The inset shows the two upper curves (filled circles and open triangles) as a function of $\Delta\tau^2$ over an expanded $\Delta\tau$ range. For the QMC_2 (filled circles) it also compares the mixed quadratic/cubic fit (solid line) with a purely quadratic fit to the data points which fulfill $\Delta\tau U_f/2 \leq 0.4$ (dotted line).

$\Sigma(i\omega) = (13/14)n_f U_f + \Delta\Sigma(i\omega)$ for all frequencies at a fixed $\Delta\Sigma(i\omega)$ which is defined in the previous section. This $\Sigma(i\omega)$ yields a new n_f via Eq. (4), and so on until convergence. As can be seen, the dependence on $\Delta\tau$ is greatly reduced, as is also the case for the QMC_2 implementation of Section II C 1 (filled circles) which also uses this self-consistent treatment of the HF part of the the self-energy. To avoid a large $\Delta\tau$ error, the large frequency part of the self-energy and especially the constant HF part is important to the energy, and must be self-consistently correct.

The inset of Figure 1 shows the top two curves in an expanded scale versus $\Delta\tau^2$, which indicates 0.035 eV agreement between the two QMC methods in the limit $\Delta\tau \to 0$. We believe that effects of Matsubara cutoff are largely eliminated here and that Trotter errors predominate in these curves, which are expected to be of leading order $\Delta\tau^2$, at least for the QMC calculation of lattice models without the DMFT self-consistency complication.[31,44] In order to keep the Trotter errors under control, it is recommended that $\Delta\tau$ be constrained to $\Delta\tau U_f/2 < 1$,[31] and we have done so in this work. In fact at small volumes where the Trotter corrections are the largest, we would find the need to use three terms over this full range, with both $a + b\Delta\tau^2 + c\Delta\tau^3$ and $a + b\Delta\tau + c\Delta\tau^2$ providing reasonable fits to the energy. We find the ratio c/b to be significantly smaller for the first choice, which is consistent with the expectations of a leading $\Delta\tau^2$ dependence. In our DMFT(QMC_2) calculations we have therefore chosen to use the two term fit $a + b\Delta\tau^2$, however, over a reduced range. The dotted line in the inset of Fig. 1, for example, suggests that $\Delta\tau U_f/2 \leq 0.4$ might be a reasonable range for this fit, given $U_f = 5.05\,\text{eV}$ for the volume in the figure. The two-term fit also makes more sense in the volume range of the transition, where the Trotter corrections are smaller, but there is also more scatter as a function of $\Delta\tau$.

In DMFT(QMC_2) calculations for the whole volume grid we have used at least 1, 2, and 3 $\Delta\tau$ values for temperatures greater than, equal to, and less then 0.544 eV, respectively. In the first case it is easy to take $\Delta\tau$ so small that really no extrapolation is needed, or maybe one other value as a spot check at the smallest volume. At $T = 0.054\,\text{eV}$ (632 K) we used $\Delta\tau U_f/2 = 0.417$, 0.334, and 0.209.[50] Our calculations at $T = 0.027\,\text{eV}$ (316 K) were limited by expense to systematically larger values, $\Delta\tau U_f/2 = 0.667$, 0.477, and 0.334, so that extrapolations to $\Delta\tau = 0$ are more uncertain. Even the smallest $\Delta\tau$ here, which corresponds to $\Lambda = 320$, leads to a $\Delta\tau^2$ value that is 2.6 times larger than its counterpart at $T = 0.054\,\text{eV}$. Fortunately, we see every indication that our electronic Hamiltonian is already very close to its low-temperature limit by $T = 0.054\,\text{eV}$ (632 K), as these total energies agree with those at $T = 0.027\,\text{eV}$ within their error bars at the same *finite* $\Delta\tau$ values. The $\Delta\tau \to 0$ extrapolations are more benign for n_f and d which also agree well for the two temperatures. Accordingly, we do not display the $T = 0.027\,\text{eV}$ results in this paper, but do comment on the agreement between the two temperatures as specific quantities are presented.

We have alluded earlier to the fact that the Trotter approximation errors get larger at smaller volume in the present work. This makes sense as these are related to the commutator of the kinetic and potential energies, and should thus depend on the size of the hybridization, which gets larger as volume is reduced. We find no discernible dependence of the energy on $\Delta\tau$ for volumes in the γ phase of Ce for the range of Λ investigated, but that for the smaller volume α phase, we find $dE/d\Delta\tau^2$ to become significant and to increase in magnitude with decreasing V. Since the γ–α transition is intrinsically related to the growing importance of hybridization versus the Coulomb interaction as volume is decreased, this behavior is perhaps not surprising, although the effect turns on rather abruptly, appearing as almost another signature of the transition. Similar behavior has been seen for the periodic Anderson model.[47,48]

D. Calculation of the LDA+DMFT energy

There are several possible expressions for the DMFT total energy per site, depending on whether the potential energy is obtained using the self energy

$$E_{\rm DMFT} = \frac{T}{N}\sum_{n\mathbf{k}\sigma} {\rm Tr}\left[\{H^0_{\rm LDA}(\mathbf{k}) + \tfrac{1}{2}\Sigma(i\omega_n)\} \times G_{\mathbf{k}}(i\omega_n)\right] e^{i\omega_n 0^+}\,, \quad (13)$$

or from a thermal average of the interaction in Eq. (1)

$$E_{\rm DMFT} = \frac{T}{N}\sum_{n\mathbf{k}\sigma} {\rm Tr}\left[H^0_{\rm LDA}(\mathbf{k}) G_{\mathbf{k}}(i\omega_n)\right] e^{i\omega_n 0^+} + U_f\, d\,. \quad (14)$$

In the latter expression,

$$d = \frac{1}{2N}\sum_{\mathbf{i}} {\sum_{m\sigma,m'\sigma'}}' \langle \hat{n}_{\mathbf{i}fm\sigma}\, \hat{n}_{\mathbf{i}fm'\sigma'}\rangle \quad (15)$$

is a generalization of the one-band double occupation for multi-band models, which may be calculated directly in the QMC presuming the site average is given by the associated impurity problem. If we were using the *exact*, **k**-dependent self-energy in these equations, Eq. (13) would be equivalent to Eq. (14) and to the Galitskii-Migdal[45] expression for the total energy. We find Eq. (14) to be far superior in the present LDA+DMFT(QMC) calculations in regard to low-temperature stability and agreement with known limits, possibly not surprising in that it takes a thermal expectation of the *true* Coulomb interaction for the problem. We use Eq. (13) for the LDA+DMFT(H-I) energy in preference to Eq. (14) with a purely atomic calculation of d. However, it should be noted that for vanishing intersite hybridization at large volume, as well as at high temperatures, the H-I self-energy is exact, and indeed we find agreement between QMC and H-I results for $E_{\rm DMFT}$ in these limits.

To evaluate the total LDA+DMFT energy $E_{\rm tot}(T)$ including all core and outer electrons, we add a correction to the paramagnetic all-electron LDA energy $E_{\rm LDA}(T)$

$$E_{\rm tot}(T) = E_{\rm LDA}(T) + E_{\rm DMFT}(T) - E_{\rm mLDA}(T)\,, \quad (16)$$

which consists of the DMFT energy $E_{\rm DMFT}(T)$ less an LDA-like solution of the same many-body model Hamiltonian Eq. (1), thus "model LDA" or $E_{\rm mLDA}(T)$. The latter is achieved by a self-consistent solution of Eqs. (2) and (4) for n_f taking a self-energy $\Sigma_{\rm mLDA} = U_f(n_f - \frac{1}{2})$. From this, the kinetic energy is calculated by the first term of Eq. (14) and the potential energy by $\frac{1}{2}U_f n_f(n_f - 1)$. Note that while all of these expressions are explicitly temperature dependent,[46] the present calculations are electronic only and do not attempt to add lattice-vibrational contributions. Estimates of these contributions are similar for the α- and γ-Ce phases, however, and appear to have little impact on the phase diagram.[12]

Finally, one virtue of the Hamiltonians Eq. (1) is that it is possible to reach high-temperature limits where the entropy is precisely known. One may then calculate the entropy from the DMFT energy

$$S_{\rm DMFT}(T) = S_\infty - k_{\rm B}\int_T^\infty dT' \frac{1}{T'}\frac{dE_{\rm DMFT}(T')}{dT'}\,, \quad (17)$$

where $S_\infty = k_{\rm B}[M\ln M - n\ln n - (M-n)\ln(M-n)] = 12.057\,k_{\rm B}$, for $M = 32$ states and $n = 4$ electrons per site for Ce.

III. THERMODYNAMICS

In this section we consider thermodynamic properties of Ce, more specifically the energy, specific heat, entropy, and free energy, over a wide range of volume V and temperature T. Intercomparison of the Hartree-Fock (HF), DMFT(H-I), and DMFT(QMC) methods to solve the effective LDA Hamiltonian Eq. (1) here serves to validate all three calculations in limits where they should and do give the same answers, and also to point out shortcomings of the more approximate techniques elsewhere. Then we turn specifically to the α–γ transition in Ce, and use the total energy, Eq. (16), and entropy, Eq. (17), to present evidence for the volume collapse transition.

A. Global behavior

Figure 2 shows the correlation energy of the effective LDA Hamiltonian Eq. (1), defined as the energy E of Eq. (1) less the paramagnetic HF result $E_{\rm PMHF}$ for the same Hamiltonian. Results for polarized HF, DMFT(H-I), and DMFT(QMC) as obtained from Eqs. (13) and (14) in the last two cases, respectively, are compared in this manner for an extended range of atomic volumes at five temperatures. The polarized HF solutions assume ferromagnetic spin order, and display both spin and orbital polarization, with one band depressed below the Fermi level and the other thirteen lying above. These HF calculations (dash-dot curves) are seen to give good energies at large volume and low-temperature in comparison to the DMFT(QMC) (solid lines with data points), as has been observed previously for the Anderson Hamiltonian.[47,48] Thus, the polarized Hartree-Fock solution and other polarized static mean-field methods such as orbitally polarized LDA,[15,16,17] self-interaction-corrected LDA,[17,18,19] and LDA+U[20,21] can be expected to give good low-temperature total energies in the strong coupling limit. As the atomic volume is reduced, the difference between polarized and paramagnetic HF energy, $E_{\rm polHF} - E_{\rm PMHF}$, becomes positive near 22 Å^3, and the HF solution has a transition from the polarized to the paramagnetic solution, where all fourteen bands have coalesced together above but slightly overlapping the Fermi level. The highest two temperatures in Fig. 2 lie above

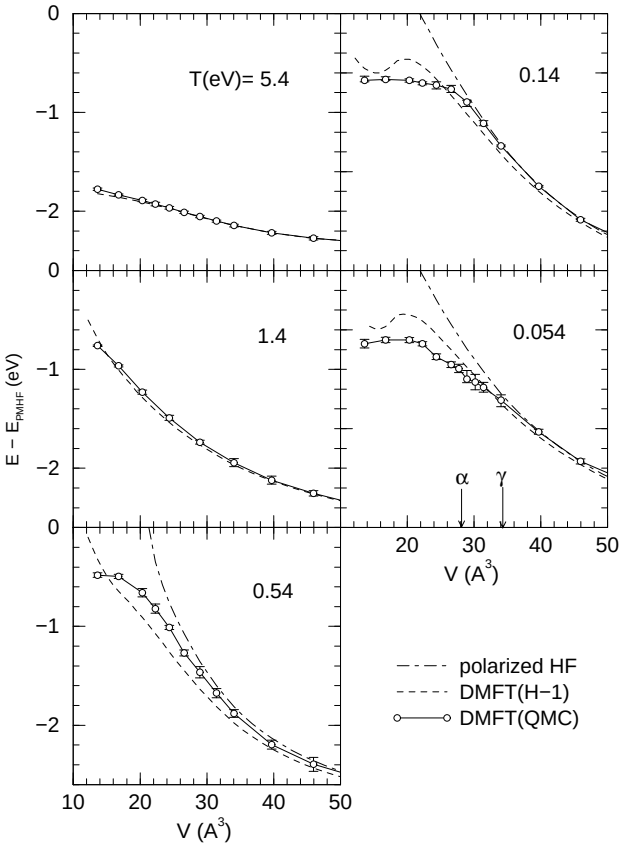

FIG. 2: Correlation energy, i.e., the difference between the LDA+DMFT and the paramagnetic HF (PMHF) energy, as a function of volume at five temperatures. At large volumes, the LDA+DMFT(QMC) energy agrees with the polarized HF and the Hubbard-I (H-I) solutions. But the LDA+DMFT(QMC) energy breaks away from the polarized HF energy for decreasing volume, leading to a region of negative curvature in the vicinity of the experimentally observed α-γ transition (indicated by arrows) at low temperature.

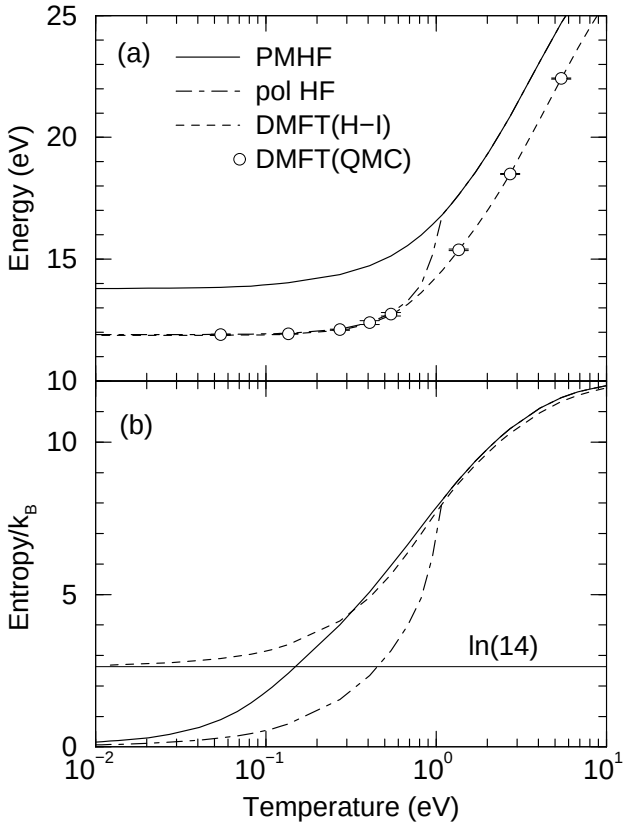

FIG. 3: Energy (upper figure) and entropy (lower figure) of the LDA+DMFT Hamiltonian Eq. (1) vs. temperature at $V = 46$ Å^3. At this relatively large volume, the DMFT(QMC) and DMFT(H-I) energies agree with each other and, at lower temperatures, also with the polarized Hartree-Fock solution. However, the entropy of the latter is completely wrong since the 14-fold degeneracy of the local magnetic moment is disregarded.

the critical point for this transition, and so there is no polarized HF solution.

Turning to the Hubbard-I approximation, which becomes exact in the atomic limit, it is no surprise that the DMFT(H-I) results (short-dashed curves) should agree well with the DMFT(QMC) energies at large volume for *all* temperatures. This approximation is also exact in the high temperature limit, as may be seen from Fig. 2, where there is also increasingly good agreement at high temperature for all volumes considered here. The agreement between the two distinct DMFT calculations in these limits provides a test of the reliability of both approaches used here.

A direct view of the temperature dependence is given in Fig. 3a where the energy E of Eq. (1) is plotted versus T for an atomic volume V of 46 Å^3. At this relatively large volume, the DMFT(QMC) and DMFT(H-I) results agree closely and smoothly interpolate between the polarized HF energy at low temperatures and the paramagnetic HF result at high temperature (above about 15 eV, not shown). There is no temperature-induced transition in the DMFT results here, in contrast to the unphysical transition from the paramagnetic to the polarized phase within HF at $T \sim 1$ eV. This transition is a shortcoming of the paramagnetic HF phase in which double-occupations of f-electrons on the same Ce site can not be avoided such that the paramagnetic (interaction) energy is too high.

Additional insight is provided by the corresponding entropy in Fig. 3b. The DMFT(H-1) entropy approaches $k_{\rm B}\ln(14)$ at low temperature, which is effectively the degeneracy of the Hund's rules magnetic moment $k_{\rm B}\ln(2J+1)$, where without intra-atomic exchange and spin orbit interaction we get the full 14-fold degeneracy of the f level rather than the proper 6-fold degeneracy for $J=5/2$. At still lower temperatures, crystal field effects are known to reduce the entropy.[49]

Figure 3 illustrates two important aspects in which HF and more rigorous techniques differ. First, the HF transition at about 1 eV corresponds to *simultaneous* moment

formation and magnetic ordering. In contrast, the two processes are distinct in more rigorous treatments, with the moment formation occurring in a continuous fashion at higher temperatures, culminating in the low-T plateau in Fig. 3b, with the onset of magnetic order (if it occurs) coming at yet lower temperatures off the scale of the plot. Second, polarized HF gives good *low-T* energies at large volumes because one of the Hund's rules multiplet states will be a single Slater determinant. However, its broken symmetry mistreats the entropy at lower temperatures, giving zero instead of, e.g., $k_{\rm B}\ln(2J+1)$ for $n_f=1$ in the atomic limit, so that the finite-T thermodynamics are incorrect.

B. Transition

We now consider thermodynamic evidence for the α–γ transition in Ce. While the QMC error bars restrict us from making a quantitative prediction, we argue that the present results do suggest the transition. Evidence is already apparent in Fig. 2, where the DMFT(QMC) correlation energy is seen to bend away from the polarized HF result as temperature is lowered, leading to a region of negative curvature in the vicinity of the observed transition (arrows). As the other terms ($E_{\rm LDA}$ and $E_{\rm PMHF}-E_{\rm mLDA}$) contributing to the total energy Eq. (16) all have positive curvature throughout the range considered in this work, this correlation contribution is then the only candidate to create a region of negative bulk modulus in the low-temperature total energy, i.e., a thermodynamic instability, and thence a first order phase transition given by the Maxwell common tangent.

Figure 4 shows total energies Eq. (16) for the DMFT(QMC) and polarized HF methods at the three lowest temperatures of Fig. 2. The region of negative curvature just noted in the correlation energy is seen to cause a substantial depression of the DMFT(QMC) total energies (solid curves with symbols) away from the polarized HF results (dashed curves) below 35 Å^3, which is most pronounced at the lowest temperature, $T=0.054$ eV. The consequent shallowness in the DMFT(QMC) curve at this temperature persists over the observed range of the two-phase region (arrows), although statistical uncertainties preclude any claim of seeing negative curvature. The slope is also consistent with a -0.6 GPa pressure (long-dashed line), which is the extrapolated transition pressure at $T=0$.[12] We suggest in fact that these $T=0.054$ eV (632 K) total electronic energies are already close to the low-T limit. Both the DMFT(H-I) and HF energies at this temperature differ by less than 0.006 eV from corresponding results at half this temperature, throughout the volume range in Fig. 4. Our DMFT(QMC) calculations at $T=0.027$ eV (316 K) are also consistent with this conclusion, as discussed in Sec. II C 2,

That the electronic contribution to the total energy might be close to its low temperature limit below about 600 K is also consistent with the analysis of the α–γ transition by Johansson *et al.*,[12] who attribute the temperature dependence of the transition pressure primarily to the difference in entropy, which is zero and $k_{\rm B}\ln(2J+1)$ for the α and γ phases, respectively. That is, for temperatures larger than both the Kondo temperature and the crystal-field splitting[49] in the γ phase, yet still fairly low (say 200–600 K), the temperature dependence of the γ-phase free energy may be dominated by the linear term $-k_{\rm B}\ln(2J+1)T$ arising from a plateau such as in Fig. 3b, while presumably the total energies (both α and γ) are closer to the low-T limit due to their faster T^2 dependence.

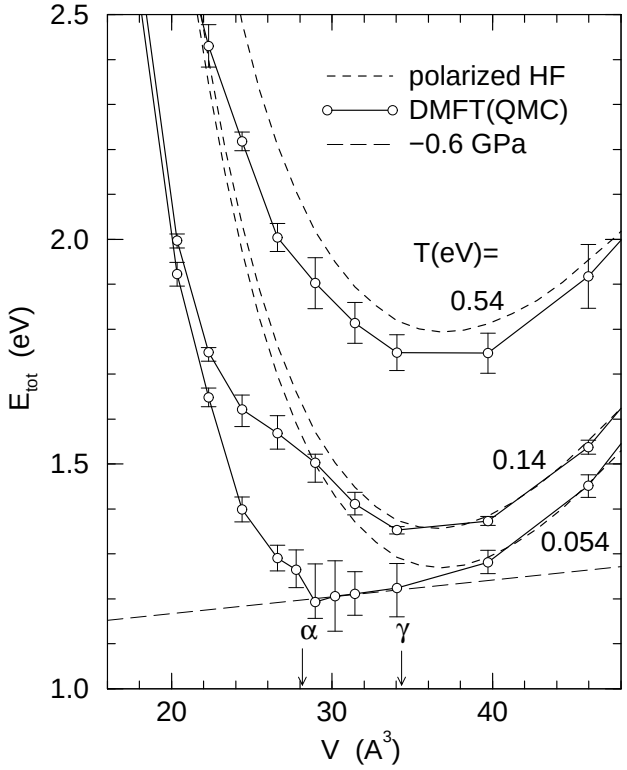

FIG. 4: Total LDA+DMFT(QMC) and polarized HF energy as a function of volume at three temperatures. While the polarized HF energy has one pronounced minimum in the γ-Ce phase, the negative curvature of the correlation energy of Fig. 2 results in the development of a side structure ($T=0.14$ eV), and finally a shallowness ($T=0.054$ eV), which is consistent with the observed α-γ transition (arrows) within our error bars. These results are also consistent with the experimental pressure given by the negative slope of the dashed line.

We have calculated both the DMFT(QMC) specific heat $C(V,T)$ and entropy $S(V,T)$ for the effective Ce LDA Hamiltonian Eq. (1). We first calculated DMFT(H-I) energies Eq. (13) on a logarithmic temperature grid up to the high-T limit ($\sim 10^3$ eV) where the entropy is known to be $12.057\,k_{\rm B}$. As noted earlier, the DMFT(H-I) method is correct at high temperatures, and indeed the DMFT(QMC) energies obtained via Eq. (14) closely approach the H-I results as T is increased, e.g., lying

above by only 0.024 and then 0.004 eV at $T = 5.4$ and 13.6 eV, respectively, for $V = 16.8\,\text{Å}^3$. We therefore fit the difference between the QMC and H-I energies at eight temperatures from 0.054 to 5.4 eV to the form $a + \sum_n b_n/(1 + n\Delta/T^2)$, $n = 1$–3, which has a T^2 behavior at low temperatures, and is benign at high temperatures. These smoothed and interpolated differences were added to the DMFT(H-I) energies to create a fine grid of "DMFT(QMC)" energies from which $C(V,T) = \partial E(V,T)/\partial T|_V$ was calculated by numerical differentiation, and $S(V,T)$ by integration down from the high-T limit according to Eq. (17). Note that while the finite nature of Eq. (1) is unphysical at very high temperatures, these results are nonetheless entirely meaningful at more modest temperatures where the omitted core and higher-lying valence states will be frozen out, e.g., below ~ 3 eV near the α–γ transition, given a spectrum of Eq. (1) that extends to nearly 30 eV above the Fermi level in that volume range.

The challenging need for accurate energy derivatives, as well as the sensitivity of Eq. (17) to the lowest temperatures given the $1/T$ factor, requires a stringent convergence criterion for the kinetic-energy Matsubara sums. Otherwise we observe unphysical negative low-T limits of the entropy for $V < 25\,\text{Å}^3$. We have also constrained the fits to smooth out the value of this low-T limit as a function of volume over this same range. In all cases it is to be emphasized that the fits give excellent representation of features in $E_{\text{DMFT(QMC)}}(T) - E_{\text{DMFT(H–I)}}(T)$, ranging in size from 0.1 to 0.24 eV upon decreasing the volume from $V = 35$ to 25 Å^3, and are well within the ± 0.03 eV error bars in the data. The same fits were used to obtain both $C(V,T)$ and $S(V,T)$.

The temperature dependence of the DMFT(QMC) specific heat is shown in Fig. 5 at six volumes. The most significant feature is the appearance of the low temperature peak in the range $T = 0.1$–0.2 eV, which coincides precisely with growth of the quasiparticle peak or Abriksov-Suhl resonance at the Fermi level in the $4f$ spectra, as will be seen in the next section. Analogous behavior has been discussed for the one-band Hubbard model.[31] The low temperature peak in the specific heat is just barely discernible at the γ-phase volume of 34 Å^3 in Fig. 5, has become rather prominent by 29 Å^3, which is slightly larger than the α-phase volume, and then continues to broaden and shift to higher temperatures as volume is further reduced. The broad peak near 1 eV which appears at all volumes is due both to the $4f$ charge fluctuations, and also to *spd*-valence to $4f$ excitations, given that n_f increases by $\sim$20% on raising the temperature to 1.4 eV. Note also in regard to the charge fluctuations that the peak in $C(T)$ should occur at significantly smaller T than the Coulomb repulsion $U_f \sim 6$ eV, as may be seen in the case of the half-filled one-band Hubbard model. Here, the specific heat peak occurs at $T = 0.208\,U$ in the absence of hopping $t = 0$, and the location of the peak is also depressed by the band width.[31]

The volume dependence of our DMFT(QMC) entropy

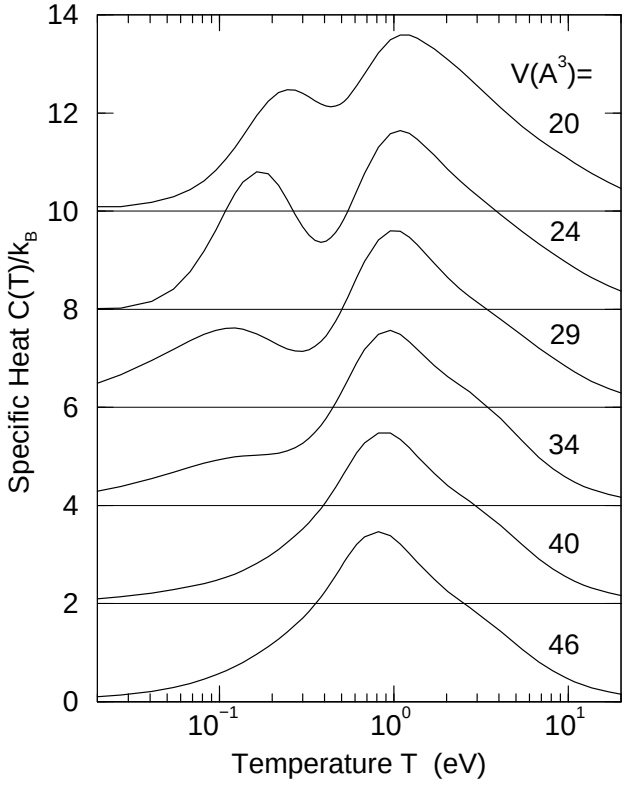

FIG. 5: Specific heat as a function of temperature for different volumes (off-set as indicated). At smaller volumes, an additional low-energy peak develops, coinciding with the formation of an Abrikosov-Suhl resonance (see Fig. 8 below).

is shown in Fig. 6 for six temperatures. The rapid increase in the entropy over the α–γ transition (28.2–34.4 Å^3) is due precisely to the low temperature peak peak in $C(T)$, which contributes to the entropy via its weighted area $\int dT C(T)/T$. Thus, at large volumes where the $4f$ spectral weight is Hubbard-split with no contribution at the Fermi level, the low-T entropy is pinned at $k_{\text{B}} \ln(2J+1)$ (ignoring effects of crystal field at yet lower T). Then, as the volume is reduced, the quasiparticle peak begins to grow at the Fermi level, the weighted area of its associated heat capacity peak reduces the low-T entropy below $k_{\text{B}} \ln(2J+1)$ via Eq. (17). The physical interpretation is of course that the degeneracy associated with the $2J+1$ directions of the Hund's rules moment disappears as this moment is either screened or collapses on reducing the volume.

For completeness, we conclude this section by providing the free energy $F = E_{tot} - ST$ in Fig. 7, although the uncertain errors in the entropy, and the fact that the large-V, low-T value is 50% too large [taking into account the spin-orbit coupling will give $k_{\text{B}} \ln(6)$ instead of $k_{\text{B}} \ln(14)$]. Given that the electronic total energy E_{tot} is near its low-T limit by $T = 0.054$ eV, we consider that curve as "$T = 0$", and then include it again as $F = E_{tot} - ST$ for $T = 0.054$ eV. The error bars on all

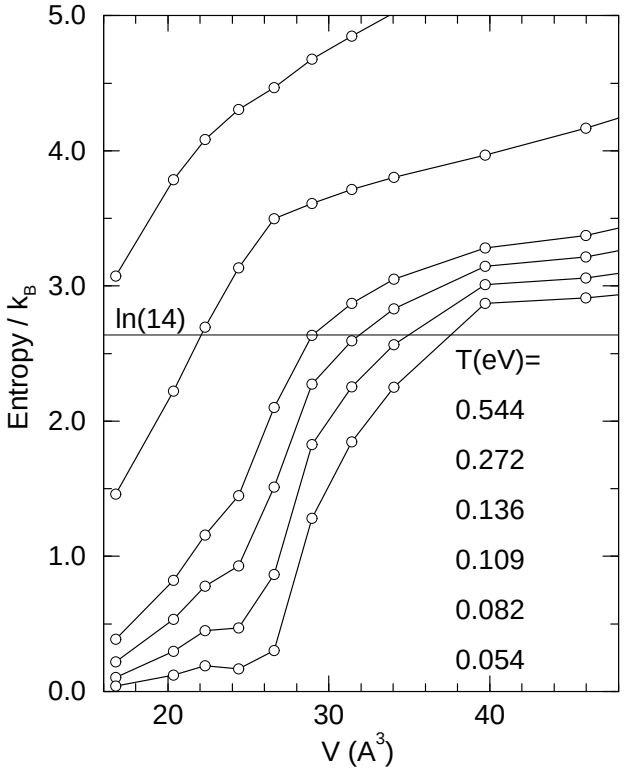

FIG. 6: Entropy as a function of volumes for different temperatures. In the vicinity of the α-γ transition (28.2-34.3 Å^3), the entropy increases rapidly.

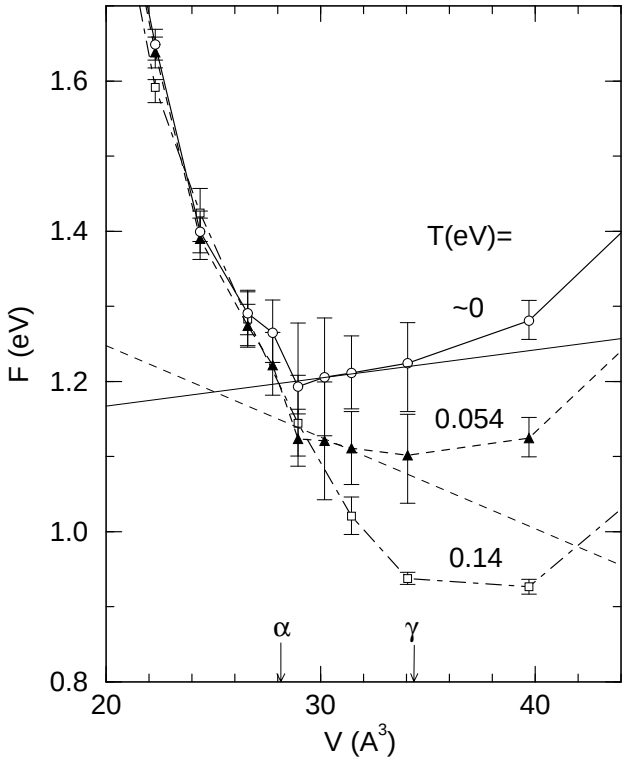

FIG. 7: Free energy as a function of volume at three temperatures, compared to lines whose negative slopes give the experimental α-γ transition pressures at $T=0$ (solid line) and 0.054 eV (dashed line). Given the statistical uncertainties, the results are consistent with experiment and show that a shift of the α-γ transition volumes is primarily due to the entropy.

curves are just from the energy. The slopes of the two straight lines give the experimental transition pressures at $T=0$ and 0.054 eV, and arrows mark the observed boundaries of the α–γ transition at room temperature. The essential conclusion of Fig. 7 is that these results are consistent with experiment, though stronger claims are precluded by the statistical uncertainties. Nonetheless, the results of this section which we find compelling are the way in which $E_{tot}(V)$ systematically develops a shallowness in the vicinity of the α–γ transition as temperature is lowered, and the structure in the specific heat and entropy.

IV. SPECTRA

In this section, we discuss the spectral changes through the α-γ transition. To obtain the physical spectrum $A(\omega) = -\frac{1}{\pi}\mathrm{Im}G(\omega)$, one has to analytically continue the QMC data from the imaginary time (Matsubara frequency) representation to real frequencies ω:

$$G(\tau) = \int_{-\infty}^{\infty} \mathrm{d}\omega \, \frac{e^{\tau(\mu-\omega)}}{1+e^{\beta(\mu-\omega)}} A(\omega). \qquad (18)$$

As one can see in Eq. (18), the values of $A(\omega)$ at large (positive or negative) frequencies affect $G(\tau)$ only weakly because the integral kernel is exponentially small in this regime. To deal with this ill-conditioned problem which is particularly cumbersome in the presence of the statistical QMC error, we employ the maximum entropy method.[40] When interpreting the results later on, we have to keep in mind, however, that there is a significant error at larger frequencies which tends to smear out fine features such that, e.g., inner structures of Hubbard bands are not necessarily resolved. In section IV A, we present the spectra of the f- and valence-electrons of fcc Ce as a function of volume and discuss the changes at the α-γ transition. The spectra obtained are compared to photoemission and Bremsstrahlung experiments in Section IV B.

A. Change of the spectra at the α-γ transition

In Section III we noted a region of negative curvature in the correlation energy at volumes consistent with the experimental α- and γ-volumes, leading to a shallowness in the total energy and suggesting a first order phase transition at lower temperatures. To further elucidate the nature of the ongoing changes, we study the evolution of the f-electron spectrum as a function of volume for fcc Ce at $T=0.054$ eV (632 K) in Fig. 8. This temperature

is close to the critical endpoint ($T = 600 \pm 50\,\mathrm{K}$) at which the first order α-γ transition disappears experimentally.[4] From the continuous evolution of the energy versus volume curves, we expect, however, similar changes above the critical endpoint, which are not yet strong enough to cause a first order phase transition. At a very small volume, $V = 20\,\text{Å}^3$, most of the spectral weight is seen to be in a big quasi particle peak or Abrikosov-Suhl resonance at the Fermi energy, but some spectral weight has already been transferred to side structures which would be interpreted as upper and lower Hubbard bands in a Hubbard model. Moving closer to the α-γ transition (between 28.2 and 34.4 Å^3 at room temperature), the α-Ce-like spectra at $V = 29\,\text{Å}^3$ shows this three peak structure to become more pronounced with a sharp Abrikosov-Suhl resonance and well-separated Hubbard bands. The spectral weight of the Abrikosov-Suhl resonance is further reduced and smeared out when going to the γ-phase ($V = 34\,\text{Å}^3$) and finally disappears at large volumes ($V = 46\,\text{Å}^3$), at least at $T = 0.054\,\mathrm{eV}$.

Altogether, we observe, as a function of volume, the crossover from a structure which differs only slightly from a one-peak structure, to a three peak structure, and finally to a two peak structure. The physical interpretation is that the f-electrons are somewhat correlated at low volumes, where the large quasiparticle peak above the Fermi energy resembles (to a first approximation) the one-peak structure of the uncorrelated one-particle theory or the LDA. At larger volumes, the system is highly correlated, there is a magnetic moment imposed by the electrons in the lower Hubbard band, but the f-electrons at the Fermi energy are still itinerant. Finally at the largest volumes, the f-electrons are localized and the local magnetic moment is fully developed. Here, the most dramatic change of the weight of the quasiparticle peak coincides with the observed region of negative curvature in the correlation energy. We thus conclude that the drastic reduction of the weight of the quasiparticle peak is related to the energetic changes in the correlation and total energies which are consistent with the first order α-γ transition.

These features and also the three peak (Kondo-like) structure of the α and γ phases agree with the Kondo volume collapse scenario.[22] On the other hand, many-body calculations show that the behavior of the Anderson and Hubbard models — paradigms for the Kondo volume collapse[22] and Mott transition[11] scenarios, respectively — are remarkably similar in regard to their spectra and other properties at finite temperatures.[26] One important difference, however, is the absence of spectral weight at the Fermi level in the "large volume" phase of the Mott-Hubbard transition, as for example in V_2O_3,[36] in contrast to the reduced but still extant spectral weight in our γ-Ce results and the experiment,[5] which is a more Kondo-like feature.

In Fig. 9, we compare the $4f$-spectrum in the α and γ phases to results at higher temperatures ($T = 0.14\,\mathrm{eV}$) from Ref. 34. Most notably, the Abrikosov-Suhl resonance in the α-phase ($V = 29\,\text{Å}^3$) becomes much sharper when going from $T = 0.14\,\mathrm{eV}$ to $0.054\,\mathrm{eV}$. The reason for this is that the Abrikosov-Suhl resonance is smeared out thermally at $T = 0.14\,\mathrm{eV}$ (1580 K) since this temperature is comparable to the Kondo temperature, which we estimate to be $0.18\,\mathrm{eV}$ (2100 K) from the full width at half maximum [LDA+DMFT(NCA) calculations yield 1000 K, see Ref. 32]. This Kondo temperature is only a crude estimate which might also be somewhat reduced if the spin orbit coupling, which splits off states from the Fermi energy, is taken into account. Nonetheless, it reasonably agrees with experimental estimates of $T_\mathrm{K} = 945\,\mathrm{K}$ and 1800–2000 K for the Kondo temperature obtained from electronic[5] and high-energy neutron spectroscopy[51], respectively. In contrast, the peak in the γ phase remains smeared out such that one would assume a Kondo temperature lower than $0.054\,\mathrm{eV}$ (632 K); the experimental estimates are $T_\mathrm{K} = 95\,\mathrm{K}$ (Ref. 5) and 60 K (Ref. 51). The changes in the rest of the spectrum are much less

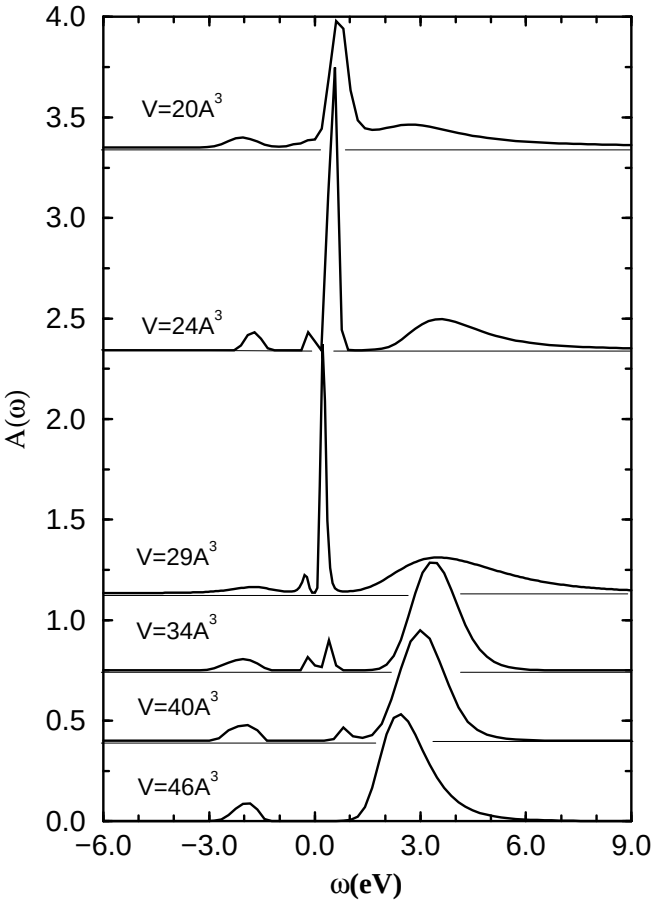

FIG. 8: Evolution of the $4f$ electron spectrum with volume at $T = 632\,\mathrm{K}$; off-set as indicated. When going from small to large volume, the weight of the central Abrikosov-Suhl resonance decreases and practically fades away at the α-γ transition from $V = 29$ to 34Å^3 . The residual weight around the Fermi energy at $V = 34\text{Å}^3$ indicates a smeared out Abrikosov-Suhl resonance as is to be expected if the Kondo temperature of γ-Ce is below $T = 632\,\mathrm{K}$.

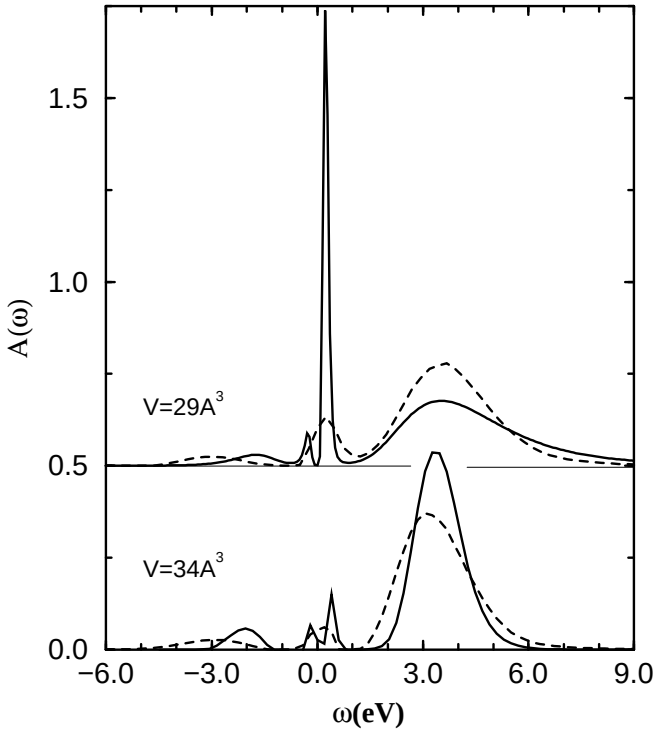

FIG. 9: $4f$ electron spectrum for α-Ce ($V = 29\text{Å}^3$) and γ-Ce ($V = 34\text{Å}^3$) at two temperatures ($T = 632\,\text{K}$: solid line; $T = 1580\,\text{K}$: dashed line). The Abrikosov-Suhl resonance of α-Ce is smeared out when increasing the temperature from $T = 632$ to $1580\,\text{K}$, indicating that the Kondo temperature is in between.

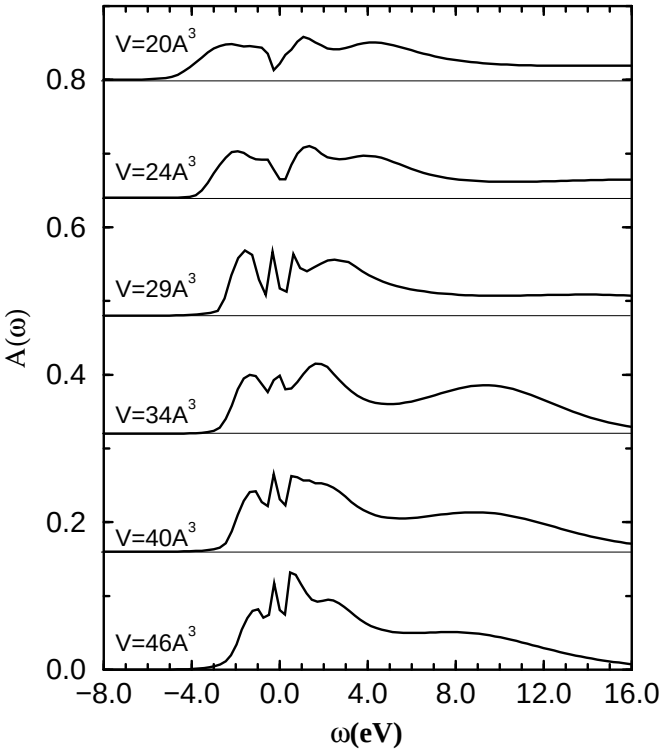

FIG. 10: Evolution of the *spd* electron spectrum with volume at $T = 632\,\text{K}$; off-set as indicated. Note the wider energy window in comparison to Figs. 8 and 9. The main effect to be seen is the decrease of the bandwidth upon increasing the volume.

dramatic. The position of the upper Hubbard band is fixed while the lower Hubbard band, which has a very small spectral weight, moves closer to the Fermi energy upon decreasing the temperature.

While the f-electrons undergo a transition from itinerant character at low volumes with a quasiparticle resonance at the Fermi energy, to localized character at larger volumes without such a resonance, the (*spd*) valence electrons remain metallic at all volumes. This can be seen in Fig. 10, which shows the valence spectral function $A(\omega)$ averaged over the *spd*-orbitals. It is finite at the Fermi energy for all volumes, such that Ce is always a metal. The biggest change in the spectrum is the decreasing valence bandwidth when increasing the volume, which is simply due to the reduced overlap of the valence orbitals as inter-atomic distances increase. The effect of electronic correlations is less obvious. But, one can note a dip in the valence spectrum in the vicinity of the Fermi energy which is to be expected to coincide with the Abrikosov-Suhl resonance in the f-spectrum. This dip is most pronounced at lower volumes where the f-electron Abrikosov-Suhl resonance has most spectral weight.

B. Comparison to experiment

The LDA+DMFT(QMC) calculation of fcc Ce suggests a volume collapse approximately at the experimental volumes. To further test whether this theory actually describes fcc Ce, we now compare our α- and γ-Ce spectra with photoemission spectroscopy (PES)[52] and Bremsstrahlung isochromatic spectroscopy (BIS).[53] To this end, we combined the f and *spd* spectra of Section IV A with areas normalized to 14 and 18, respectively, to yield the full *spdf* density of states, and smoothed it with the experimental resolution of approximately 0.4 eV.

The comparison is shown in Fig. 11 for α and γ Ce. Although there are no free parameters in our LDA+DMFT(QMC) results,[54] the agreement between theory and experiment is very good. Particularly good is the agreement of the spectrum around the Fermi energy for both α *and* γ Ce; this part of the spectrum consists of the Abrikosov-Suhl resonance of the f-electron spectrum and the valence spectrum. Also the position of the upper and lower Hubbard bands and the relative weight of these peaks and the Abrikosov-Suhl resonance is correctly predicted by the theory. Less good is the agreement with respect to the width of the upper Hubbard band which is too narrow in our theory; the experimental upper Hubbard bands extend to energies 1–2 eV higher than our

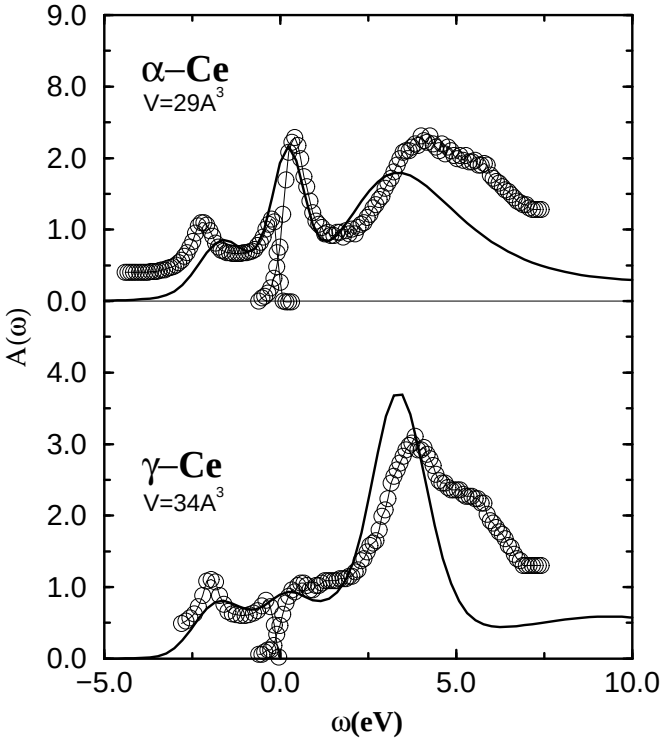

FIG. 11: Comparison of the LDA+DMFT(QMC) spectra with experiment (circles)[5]. Although there are no free parameters in the calculated spectrum, the agreement is very good, in particular at the Fermi energy($\omega = 0$). The additional structure in the upper Hubbard band which is seen in the experiment is likely due to the exchange interaction which was neglected in our calculation.

theory. As has been argued in Ref. 32, this can be understood by the Hund's rules exchange coupling which has not been taken into account in our calculation. We justified this by noting that the exchange coupling is only effective if there are more than two electrons on one Ce site which happens only rarely. However, the excited states of the upper Hubbard-band correspond to just such double occupied states. For these, the Hund's rules coupling becomes important and will split the upper Hubbard band into multiplets. With this shortcoming resolved, the comparison to the experimental spectrum suggests that our LDA+DMFT(QMC) calculation describes α and γ Ce very well.

The α and γ spectra of previous LDA+DMFT(NCA) calculations by Zölfl *et al.*[32] are considerably different from ours and the experimental spectra, in particular the weight of the upper Hubbard bands was much higher in Ref. 32. The temperature of Ref. 32 is very close to ours ($T = 580$ K) and also the $4f$-electron Coulomb interaction value U_f is comparable, at least for the γ phase; Zölfl *et al.* employed a fixed value of $U_f = 6$ eV whereas the constrained LDA values in our calculations are $U_f = 5.72$ eV and 5.98 eV for α and γ Ce, respectively. In view of this we tend to explain the differences, at least for γ-Ce, by the different method employed to solve the DMFT equations, in particular, since the non-crossing approximation (NCA) is a resolvent perturbation theory for strong coupling.

V. LOCAL MOMENT AND $4f$ OCCUPATIONS

Important additional information about the α-γ transition and the effects of electron correlation in Ce are contained in the number of $4f$ electrons per site n_f, the double occupation d, and quantities derived from these such as the fraction of sites $w(f^n)$ with $n = 0,1,2$ f electrons, and the local magnetic moment. These parameters can discriminate between the various models, as for example the promotional model[10] assumes a considerable change in the number of $4f$ electrons at the α-γ transition, in contrast to the Kondo Volume collapse[22] and Mott transition[11] scenarios which do not. The latter two on the other hand distinguish themselves by assuming a small and large change of the magnetic moment, respectively.

Figure 12 gives n_f as a function of volume at four temperatures.[55] The lowest curve at $T = 0.054$ eV (632 K) is already very close to the low-T limit, as our results at half this temperature are the same to within generally 0.004, or at most 0.01 electrons per site. There are two main tendencies: With decreasing V, n_f increases due to the upward motion of the $6s, p$ levels relative to the $4f$ level under compression; it also increases with T due to the thermal occupation of the large $4f$ density of states lying above the Fermi level. Superimposed on this behavior is, at low temperatures, an abrupt reduction of n_f in the observed two-phase region (marked) as volume is reduced, an anomaly which is annealed away by $T = 0.5$ eV similar to the case of the total energy. This effect leads to a number of $4f$ electrons close to one, ruling out the promotional model[10] and suggesting Kondo physics given the sharp quasiparticle peak seen in the previous section. Quantitatively, we get a 4% reduction in n_f across the two-phase region from 1.035 ± 0.017 to 0.993 ± 0.010 at $T \leq 0.054$ eV. Similar behavior is seen in the 10% drop from 1.014 to 0.908 of Zölfl *et al.*[32] in their LDA+DMFT(NCA)calculations, and the 11% reduction from 0.971 ± 0.006 to 0.861 ± 0.015 electrons/site of Liu and coworkers,[5] who fitted a single impurity Anderson model to the experimental $4f$ spectrum. The reason for the drop in n_f is a systematic increase in the double occupation d under compression. Since d is the potential energy divided by U_f, the energy cost associated with increasing d can be ameliorated by reducing n_f.

Since there is little chance of more than doubly-occupied sites in Ce at low temperature, n_f and d provide sufficient information to obtain the fractions of sites with

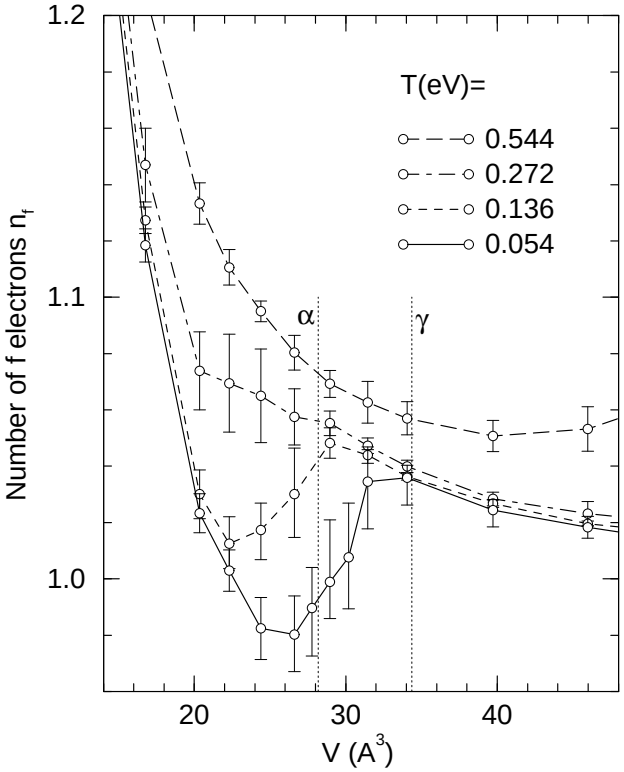

FIG. 12: Number of $4f$ electrons n_f vs. volume at four temperatures. At low temperatures and in the vicinity of the α-γ transition, n_f is very close to one.

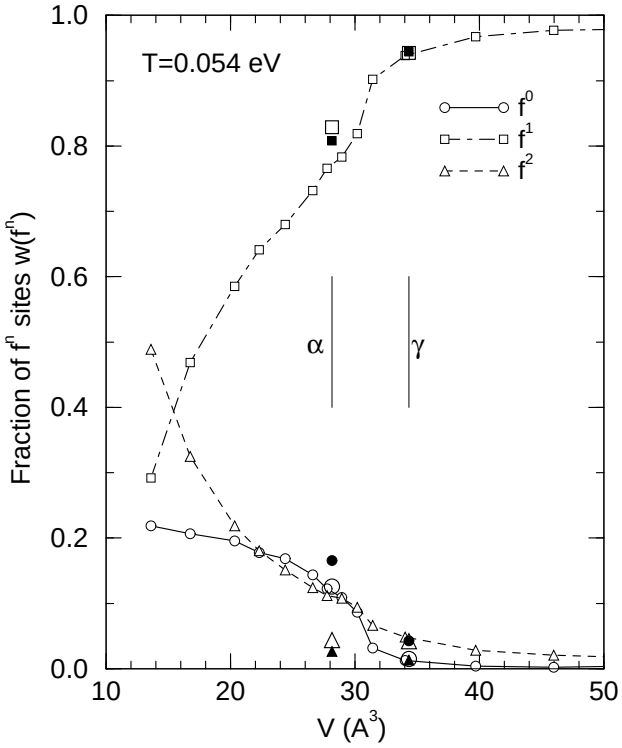

FIG. 13: Fraction of empty (f^0), singly (f^1), and doubly occupied sites (f^2) vs. volume as calculated by LDA+DMFT (QMC) (open symbols with lines) at $T = 0.054\,\mathrm{eV}$ in comparison to LDA+DMFT(NCA) (large open symbols)[32] and impurity Anderson model results (filled symbols).[5] While the DMFT results agree very well for the γ phase, there are significant differences in the α phase as discussed in the text.

various integral f^n occupations.

$$\begin{aligned} w(f^0) &= 1 - n_f + d \\ w(f^1) &= n_f - 2d \\ w(f^2) &= d \end{aligned} \tag{19}$$

Fig. 13 shows our DMFT(QMC) results for these weights at $T = 0.054\,\mathrm{eV}$, which are also close to the low-temperature limit. At large volume one sees that each site nearly always has one f electron, and that empty or doubly occupied sites are rare, as would be expected for $n_f \sim 1$ in the absence of significant hybridization to move these electrons to either f or v (*spd* valence) states on neighboring sites. For the f electrons to begin to move around from one site to another in any independent fashion under the influence of larger ff hybridization, or for there to be virtual charge fluctuations of the form $f^1v^3 \rightarrow f^0v^4$ and $f^1v^3 \rightarrow f^2v^2$ due to increased fv hybridization, it is clear in each case that both empty and doubly occupied sites must become more common at the expense of singly occupied sites if the volume is reduced, as evident in Fig. 13. Note that these changes are especially dramatic over the experimental two phase region (marked).

The filled symbols in Fig. 13 show the impurity Anderson model results of Liu *et al.*[5] at the observed α- and γ-Ce volumes; the large open symbols, the DMFT(NCA) results of Zölfl and coworkers.[32] Our DMFT(QMC) values are $w(f^0), w(f^1), w(f^2) = 0.013 \pm 0.019$ (0.118 ± 0.025), 0.939 ± 0.028 (0.771 ± 0.033), and 0.048 ± 0.009 (0.111 ± 0.008) for the γ (α) volumes, respectively. The two DMFT calculations agree well within these uncertainties for all three populations $w(f^n)$ at the larger γ-phase volume, and also with the impurity Anderson model value for $w(f^1)$; although for the two small populations, they obtain $w(f^0) < w(f^2)$ in reverse order to the values of Liu and coworkers.[5] The most significant difference at the α-Ce volume is the rather larger double occupancy, $d = w(f^2) = 0.111 \pm 0.008$, obtained by our DMFT(QMC) calculations in comparison to smaller values 0.044 and 0.026 obtained by the the DMFT(NCA) and impurity Anderson model, respectively. Temperature is unlikely to be a factor here, as we obtain n_f and d unchanged within our error bars at half the temperature of the DMFT(QMC) results in Fig. 13, e.g., $d = w(f^2) = 0.108 \pm 0.008$ at $T = 0.027\,\mathrm{eV}$ (316 K).

There are some differences between the three calculations, however, which might account for differing $w(f^n)$ predictions: (i) Our calculated Coulomb interaction for α-Ce, $U_f = 5.7\,\mathrm{eV}$, is slightly smaller than the $U_f = 6\,\mathrm{eV}$ employed in Refs. 32 and 5. (ii) Liu *et al.* employ an

impurity Anderson model whereas both we and Zölfl *et al.* extract a periodic Anderson type of model from the LDA, including f-f hybridization. While we also deal with an Anderson impurity model in the course of our DMFT solution, this impurity model is only an auxiliary construction with a complicated and strongly renormalized (non-constant) hybridization. (iii) Finally, in contrast to the DMFT(QMC), both DMFT(NCA)[32] and the $1/N$ approach[56] of Ref. 5 are based on perturbation expansions in the hybridization strength, a quantity which gets larger with reduced volume. Thus, while these two approximations are controlled by the smallness of the hybridization strength and also by $1/N$ (we have $N=14$ f orbitals), there are nonetheless larger corrections when the hybridization is increased, i.e., when going to the more itinerant α-Ce. Note in this context that the ratio of Coulomb interaction to an effective bandwidth determined by the total f-f and f-valence hybridization changes from 3.8 to 2.5 across the γ-α transition.[3]

It is possible to quantify the degree of f-electron correlation by noting certain limiting values of d. A natural minimum is provided by the strongly correlated ground state of Eq. (1) in the atomic limit, where d is a piecewise linear function of n_f, with $d=d_{\min}=\max(0,n_f-1)$ for $n_f \leq 2$. Similarly, $d_{\max}=(13/28)n_f^2$ from Eq. (15) in the uncorrelated limit $\langle \hat{n}_1 \hat{n}_2 \rangle = \langle \hat{n}_1 \rangle \langle \hat{n}_2 \rangle$, which is approached for volume $V \to 0$ leading to a vanishing ratio of Coulomb interaction to bandwidth. Fig. 14 shows a plot of the ratio $(d_{\max}-d)/(d_{\max}-d_{\min})$ for the present Ce calculations at $T=0.054\,\mathrm{eV}$, which reflects strong and weak correlation limits at 1 and 0, respectively. Note the polarized to paramagnetic HF transition at $V \sim 20\,\text{Å}^3$ for decreasing volume, and the fact that the paramagnetic HF result is completely uncorrelated ($d \approx d_{\max}$) as expected. The fact that the d ratio in this case is not precisely zero is due to a small amount of orbital polarization arising from the fact that $4f$ bands of different symmetry overlap the Fermi level to slightly different extent, whereas $d_{\max}$ was defined for all spin-orbital occupations to be $n_f/14$.

The combination of increasing d and decreasing n_f causes a sharp decrease in correlation (delocalization) of the DMFT(QMC) result for decreasing volume through the observed γ-α transition (marked), in agreement with tenets of the Mott-transition model.[11,57] The value of the DMFT(QMC) d ratio is 0.76 ± 0.08 at the α volume, combining all of the uncertainties in both d and n_f. While this value is certainly less correlated than the DMFT(NCA)[32] (large open circles) and impurity Anderson model[5] (filled circles) predictions at 0.89 and 0.92, respectively, it is far from the kind of uncorrelated behavior seen in the paramagnetic HF of Fig. 14 or, presumably also, in the LDA. Even at the smallest volumes considered, the DMFT(QMC) d ratio still suggests the presence of significant correlation, which is entirely consistent with the remnant Hubbard side bands in this range as discussed in the previous section. Most notable in the DMFT(H-I) curve is a glitch at about $V=17\,\text{Å}^3$ which is

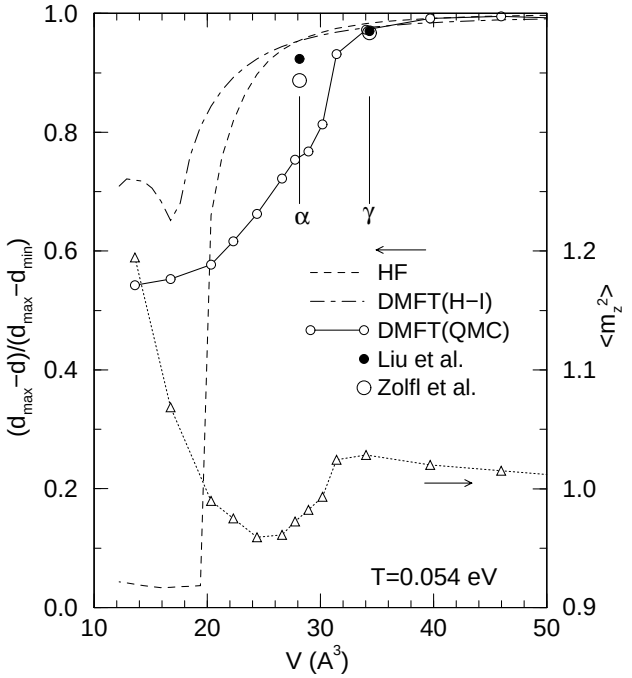

FIG. 14: Double occupation ratio $(d_{\max}-d)/(d_{\max}-d_{\min})$ and local magnetic moment $\langle m_Z^2 \rangle$ (triangles) as a function of volume at $T = 0.054\,\mathrm{eV}$. In the former case, we compare the LDA+DMFT(QMC) results with our HF and LDA+DMFT(H-I) results as well as with the LDA+DMFT(NCA) by Zölfl *et al.*[32] and the Anderson model calculations by Liu et al.[5] The double occupancy increases when going from γ- to α-Ce (experimental volumes as indicated), i.e., the electrons become more itinerant or less correlated. This effect is most pronounced in our LDA+DMFT(QMC) results; however, the d ratio is still far from the uncorrelated value $d=d_{\min}$, i.e., α-Ce is still strongly correlated.

a consequence of the behavior in n_f (not shown): Within DMFT(H-I), n_f is pinned at 1 for decreasing volume until $V=17\,\text{Å}^3$, at which point it increases and the system becomes mixed valent.

Turning to the local magnetic moment, our approximations [neglect of spin orbit, intra-atomic exchange, and the $4f$ crystal field splitting in Eq. (3)] have more serious implications for this quantity than others, and so we can provide only an estimate. Consistent with these approximations we take

$$\langle \hat{n}_{ifm\sigma} \hat{n}_{ifm'\sigma'} \rangle = \begin{cases} n_f/14 & \text{if } m\sigma = m'\sigma' \\ d/91 & \text{if } m\sigma \neq m'\sigma' \end{cases}, \tag{20}$$

such that the local magnetic moment becomes

$$\langle m_z^2 \rangle \equiv \sum_m \langle (\hat{n}_{ifm\uparrow} - \hat{n}_{ifm\downarrow})^2 \rangle = n_f - (2/13)\, d, \tag{21}$$

indicating whether a local spin moment exists. Note that this quantity does not contain information about long-range magnetic order, aside from the fact that a finite moment would be required for such order. Also note that

$\langle m_z^2\rangle$ is unlikely to vanish. Even if one just statistically distributes electrons with arbitrary i, m, and σ, some sites will have electrons with the same spin and thus $\langle m_z^2\rangle$ will be finite, but it will be smaller than its maximal value obtained in the localized regime where d is minimal.

The spin, orbital, and total angular momentum expectations can be expressed as $\langle \hat{S}_{if}^2\rangle = (3/4)\langle m_z^2\rangle$, $\langle \hat{L}_{if}^2\rangle = 12\langle m_z^2\rangle$, and $\langle \hat{J}_{if}^2\rangle = (51/4)\langle m_z^2\rangle$ due to the degeneracies in Eq. (20). Note that in the atomic limit ($n_f \sim 1$, $d \sim 0$) these expressions correctly give $S_{if} = 1/2$ and $L_{if} = 3$, although $\langle \hat{J}_{if}^2\rangle$ averages over the two spin-orbit multiplets. Our DMFT(QMC) result for $\langle m_z^2\rangle$ at $T = 0.054\,\mathrm{eV}$ is also provided in Fig. 14 (bottom dotted curve with open triangles), where this quantity is seen to drop by 5% from the γ to the α volume. This may be compared to 11% and 12% drops for the DMFT(NCA)[32] and impurity Anderson model[5] calculations, respectively, based on their values of n_f and $d = w(f^2)$. High-energy neutron scattering experiments observe single-ion magnetic response from 0.8 ± 0.1 $4f$ electrons in the α phase, suggesting also that much of the local moment persists into that phase.[51] Such high-energy or "fast" probes can detect a local moment even if it appears screened out in "slower" measurements like magnetic susceptibility. Note that the, at first view unexpected, increase in the DMFT(QMC) $\langle m_z^2\rangle$ for the smallest volumes in Fig. 14 only reflects this same behavior in n_f (Fig. 12).

The persistence of a still robust (albeit slightly reduced) local $4f$ moment into the α phase as suggested here supports the Kondo Volume Collapse scenario,[22] in that the observed temperature-independent Pauli-like paramagnetism of the α phase can then arise when the valence electrons screen out these local moments. Orbitally polarized[15,16,17] and self-interaction corrected[17,18,19] LDA results suggest that the moment actually collapses to nothing in the α phase of Ce and its analog in Pr. However, these calculations really measure spin and orbital polarization analogous to $\langle m_z\rangle$, and therefore describe a loss of magnetic order in the α-like phases without providing information about the local moment itself. Indeed, there can be a local moment $\langle m_z^2\rangle$ even in the fully uncorrelated limit, as noted earlier, since $\langle m_z^2\rangle = n_f - (2/13) d_{\max} = n_f(1 - n_f/14)$ can be significant away from empty or filled bands. Note that one may have temperature-independent paramagnetism in the presence of local moments both if there is correlated Kondo screening of these moments, as noted above, as well as by Pauli's original one-electron process in which only electrons in states near the Fermi level are free to respond to the field. The latter must dominate as one approaches the uncorrelated $V = 0$ limit.

VI. SUMMARY AND DISCUSSION

We have calculated thermodynamic, spectral, and other properties of Ce metal over a wide range of volumes and temperatures using the merger of the local density approximation and dynamical mean field theory (LDA+DMFT). The DMFT self energy was generated by rigorous quantum Monte Carlo (QMC) techniques, including a new, faster implementation that has facilitated lower-temperature results and is described in detail. Our LDA+DMFT results provide a comprehensive picture of correlation effects in compressed Ce, and their fundamental role in the first-order α-γ transition. First results of this effort have been published in Ref. 34.

At large volume, we find a Hubbard split $4f$ spectrum, the associated local magnetic moment, and an entropy reflecting the degeneracy in the moment direction. This phase is well described by the Hubbard-I approximation and its energy but not its entropy also agrees with the polarized Hartree-Fock solution. As volume is reduced, a quasiparticle or Abrikosov-Suhl resonance begins to develop at the Fermi level in the vicinity of the α-γ transition, and the entropy starts to drop. At the same time, the $4f$ double occupation grows whereas the number of $4f$ electrons remains close to one. The temperature dependence of the quasiparticle peak is consistent with a significantly larger Kondo temperature in the α phase than in the γ phase, and the parameter-free LDA+DMFT spectra are in good agreement with experiment for both α- and γ-Ce. In the range where the quasiparticle peak grows dramatically, the correlation energy as a function of volume is seen to have a negative curvature. This leads to a growing shallowness in the total energy as temperature is reduced and is consistent with the first-order α-γ transition within our error bars. Our results suggest that the temperature dependence of the transition pressure is primarily due to the entropy. Finally, if the volume is reduced below that of the ambient α phase, the quasiparticle peak grows at the expense of the Hubbard side bands, yet these Hubbard side bands persist even at the smallest volumes considered.

The Mott transition[58] (MT) and Kondo volume collapse[22] (KVC) scenarios are based on the one-band Hubbard and the periodic (or more approximate impurity) Anderson models as paradigms. The classification of our results in terms of these two standard theories requires distinguishing between the more general interpretation of the MT in the many body community,[59] e.g., applied to such materials as V_2O_3,[36] and the ideas of Johansson[11] and members of the local-density functional community as applied to the f-electron metals.[15,16,17,18,19,20,21] In the former case, correlated solutions of *both* model Hamiltonians show similar features at finite temperature such as persistence into the more weakly correlated regime of the local moment and residual Hubbard splitting,[26] just as seen here for α-Ce. The similarity between the two models can be understood from the following consideration: The conduction-electrons in the periodic Anderson model are non-interacting. Thus, they only enter quadratically in the effective action and can be integrated out by a simple Gauss integration. This results in an effective one-band

model for the f electrons of the periodic Anderson model which can behave[26] very much like the Hubbard model not only at finite temperature, but, depending on the choice of f-d hybridization, also at $T=0$.

One might try to distinguish between the two scenarios by whether the transition is caused by changes of the f-f (MT) or f-valence (KVC) hybridization. But, since realistic calculations like the present include both, this distinction is rather problematic. Another difference can be addressed unambiguously, i.e., whether the low-temperature γ phase has an Abrikosov-Suhl resonance (KVC) or not (MT). We observe the former, in agreement with experiment.[5] The energy scale of this γ-Ce Abrikosov Suhl resonance is very small such that we obtain a thermally smeared out structure instead of a sharp resonance. The smallness of the energy scale also implies that the effect on the total energy is very minor. Because of this, the low-temperature energy (but not the entropy) of γ-Ce may also be adequately described by static mean field techniques like our HF calculation as well as a number of local-density functional modifications: orbitally polarized LDA,[15,16,17] self-interaction corrected LDA,[17,18,19] and LDA+U.[20,21] These approximations have a frequency-independent (static) self-energy and provide a splitting of the $4f$-band into two bands by an (artificial) symmetry breaking. While our HF calculations as well as LDA+U work[20] for Ce give a transition at too small volume, one may drive the onset of the symmetry breaking closer to the volume of the α-γ transition by reducing the the $4f$ Coulomb interaction U_f. Such a reduced interaction strength is naturally achieved within the orbitally polarized LDA calculations which omit U_f and employ the weaker intra-atomic exchange interaction to achieve the symmetry breaking.

A major point of debate between the KVC scenario and Johansson's interpretation of the MT picture is whether the α phase of Ce is strongly correlated (KVC) or not (MT). Our results suggest that α-Ce is strongly correlated with a three peak structure consisting of the two Hubbard peaks and central quasiparticle bands as in the KVC picture.[22] In contrast, the MT model as advocated by Johansson[11] and others[15,16,17,18,19,20] predicts a single peak associated with uncorrelated, band-like f electrons. We do see a rapid increase in double occupation d across the transition, which is consistent with the delocalization ideas of this MT scenario. However, the actual value of d in the α phase is far from uncorrelated, although it indicates considerably less correlation than in the KVC picture.[5] It appears that this perspective of the MT is motivated by the LDA results, and that if one were to fully take into account electronic correlations, one would also observe a correlated three-peak solution as in the Hubbard model.[26] This correlated solution would also have preformed local magnetic moments, which would be screened at small energies on the scale of the width of the Abrikosov-Suhl resonance, as in the KVC picture, whereas the uncorrelated MT solution does not develop such local moments.

Since we find a strongly correlated α phase, the question remains why the structural and volume dependence of the total energy in the α-Ce regime is so extremely well described by normal paramagnetic LDA and its gradient corrected improvements.[13,14] This point is one of the strongest arguments advanced by Johansson[11] and others[13,14,15,16,17,18,19,20] that α-Ce-like phases should be weakly correlated. A logical explanation would be that LDA may get the interactions between the quasiparticles correct but not their formation energy. The interactions are perhaps governed by the significant weight in the central Fermi-level peak which resembles the uncorrelated LDA solution, while the formation energy may involve the residual Hubbard sidebands in some way. Thus the still very significant correlation may provide only a constant contribution to the total energy in the α-Ce regime, so that the volume and structural dependence is still well represented. This would be consistent with the energy shift between α and γ phases employed by Johansson et al.[12] in their LDA-based modeling of the transition.

Acknowledgments

Work by AKM was performed under the auspices of the U. S. Department of Energy by the University of California, Lawrence Livermore National Laboratory under contract No. W-7405-Eng-48. KH acknowledges support by the Alexander von Humboldt foundation, and RTS from NSF-DMR-9985978. We are grateful for the QMC code of Ref. 31 (App. D) which was modified for use in part of the present work. We thank A. Sandvik for making available his maximum entropy code, I. A. Nekrasov for providing the digitized experimental spectra, and G. Esirgen, J. W. Allen, and O. Gunnarsson for useful discussions.

[1] U. Benedict, J. Alloys Comp. **193**, 88 (1993).
[2] W. B. Holzapfel, J. Alloys Comp. **223**, 170 (1995).
[3] A. K. McMahan, C. Huscroft, R. T. Scalettar, and E. L. Pollock, J. Comput.-Aided Mater. Design **5**, 131 (1998).
[4] D. G. Koskimaki and K. A. Gschneidner Jr., in *Handbook on the Physics and Chemistry of Rare Earths*, edited by K. A. Gschneidner Jr. and L. R. Eyring (North-Holland, Amsterdam, 1978), p. 337; J. S. Olsen, L. Gerward, U. Benedict, J. P. Itié, Physica **133B**, 129 (1985).
[5] L. Z. Liu, J. W. Allen, O. Gunnarsson, N. E. Christensen, and O. K. Andersen, Phys. Rev. B **45**, 8934 (1992).
[6] J. W. van der Eb, A. B. Kuz'menko, and D. van der Marel, Phys. Rev. Lett. **86**, 3407 (2001).
[7] G. Eliashberg and H. Capellmann, Sov. Phys. JETP **67**, 125 (1998).
[8] B. L. Davis and L. H. Adams, J. Phys. Chem Solids **25**,

379 (1964).
[9] A. V. Nikolaev and K. H. Michel, Eur. Phys. J. B **9**, 619 (1999); **17**, 12 (2000); cond-mat/0112147.
[10] L. Pauling, J. Am. Chem. Soc. **69**, 542 (1947); W. H. Zachariasen, unpublished.
[11] B. Johansson, Philos. Mag. **30**, 469 (1974).
[12] B. Johansson, I.A. Abrikosov, M. Aldén, A. V. Ruban, and H. L. Skriver, Phys. Rev. Lett. **74**, 2335 (1995).
[13] M. S. S. Brooks, B. Johansson, and H. L. Skriver, in *Handbook on the Physics and Chemistry of the Actinides*, edited by A. J. Freeman and G. H. Lander (North-Holland, Amsterdam, 1984), Vol. 1, p. 153.
[14] P. Söderlind, Adv. Phys. **47**, 959 (1998).
[15] O. Eriksson, M. S. S. Brooks, and B. Johansson, Phys. Rev. B **41**, 7311 (1990).
[16] P. Söderlind, Phys. Rev. B **65**, 115105 (2002).
[17] A. Svane, J. Trygg, B. Johansson, and O. Eriksson Phys. Rev. B **56**, 7143 (1997).
[18] A. Svane, Phys. Rev. Lett. **72**, 1248 (1994); Phys. Rev. B **53**, 4275 (1996).
[19] Z. Szotek, W. M. Temmerman, and H. Winter, Phys. Rev. Lett. **72**, 1244 (1994).
[20] I. S. Sandalov, O. Hjortstam, B. Johansson, and O. Eriksson, Phys. Rev. B **51**, 13987 (1995).
[21] A. B. Shick, W. E. Pickett, and A. I. Liechtenstein, J. Electron Spectrosc. **114**, 753 (2001).
[22] J. W. Allen and R. M. Martin, Phys. Rev. Lett. **49**, 1106 (1982); J. W. Allen and L. Z. Liu, Phys. Rev. B **46**, 5047 (1992).
[23] M. Lavagna, C. Lacroix, and M. Cyrot, Phys. Lett. **90A**, 210 (1982).
[24] N. Sivan and Z. Zinamon, Phys. Rev. B **37**, 5535 (1988).
[25] J. Lægsgaard and A. Svane, Phys. Rev. B **59**, 3450 (1999).
[26] K. Held, C. Huscroft, R. T. Scalettar, and A. K. McMahan, Phys. Rev. Lett. **85**, 373 (2000); K. Held and R. Bulla, Eur. Phys. J. B **17**, 7 (2000). Also see P. G. J. van Dongen, K. Majumdar, C. Huscroft, and F. C. Zhang, Phys. Rev. B **64**, 195123 (2001).
[27] V. I. Anisimov, A. I. Poteryaev, M. A. Korotin, A. O. Anokhin, and G. Kotliar, J. Phys. Cond. Matter **9**, 7359 (1997).
[28] A.I. Lichtenstein and M.I. Katsnelson, Phys. Rev. B **57**, 6884 (1998).
[29] For a tutorial see, K. Held, I.A. Nekrasov, G. Keller, V. Eyert, N. Blümer, A.K. McMahan, R.T. Scalettar, T. Pruschke, V.I. Anisimov, and D. Vollhardt, in *Quantum Simulations of Complex Many-Body Systems: From Theory to Algorithms*, eds. J. Grotendorst, D. Marx and A. Muramatsu, NIC Series Volume 10 (NIC Directors, Forschungszentrum Jülich, 2002), p. 175-209; cond-mat/0112079.
[30] D. Vollhardt, in *Correlated Electron Systems*, edited by V. J. Emery (World Scientific, Singapore) 57 (1993); Th. Pruschke M. Jarrell, and J. K. Freericks, Adv. Phys. **44**, 187 (1995).
[31] A. Georges, G. Kotliar, W. Krauth, and M. Rozenberg, Rev. Mod. Phys. **68**, 13 (1996).
[32] M. B. Zölfl, I. A. Nekrasov, Th. Pruschke, V. I. Anisimov, and J. Keller, Phys. Rev. Lett. **87**, 276403 (2001).
[33] For one-band DMFT(QMC) see Ref. 31 and M. Jarrell, in *Numerical Methods for Lattice Quantum Many-Body Problems*, editor D. Scalapino (Addison Wesley, 1997).
[34] K. Held, A. K. McMahan, and R. T. Scalettar Phys. Rev. Lett. **87**, 276404 (2001).
[35] S. Y. Savrasov, G. Kotliar, and E. Abrahams, Nature **410**, 793 (2001); preprint, cond-mat/0106308.
[36] K. Held, G. Keller, V. Eyert, V. I. Anisimov, and D. Vollhardt, Phys. Rev. Lett. **86**, 5345 (2001).
[37] J. Hubbard, Proc. R. Soc. London, Ser. A, **285**, 542 (1965).
[38] O.K. Andersen, Phys. Rev. B **12**, 3060 (1975).
[39] H. L. Skriver, *The LMTO Method* (Springer, Berlin, 1984).
[40] M. Jarrell and J. E. Gubernatis, Physics Reports **269**, 133 (1996).
[41] M. Ulmke, V. Janiš, and D. Vollhardt, Phys. Rev. B **51**, 10411 (1995).
[42] For the present paramagnetic treatment with the $4f$ self energy of the form $\Sigma(i\omega)I_f$, $\Sigma(\infty) = (13/14)n_f U_f$ both in the weak coupling (Hartree Fock) and strong coupling (Hubbard-I) limits. See Sec. II B for the latter case.
[43] G. Esirgen suggested using the Hartree-Fock Green function for this purpose, private communication.
[44] R.M. Fye, Phys. Rev. B **33**, 6271 (1986).
[45] V.M. Galitskii and A.B. Migdal, Sov. Phys. JETP **7**, 96 (1958); A.L. Fetter and J.D. Walecka, *Quantum Theory of Many-Particle Systems* (McGraw-Hill, New York, 1971), Sec. 7.
[46] We use a perturbative expression for $E_{\rm LDA}(T) - E_{\rm LDA}(0)$ based on the $T = 0$ eigenvalues, c.f., A.K. McMahan and M. Ross, Phys. Rev. B **2**, 718 (1977).
[47] C. Huscroft, A. K. McMahan, and R. T. Scalettar, Phys. Rev. Lett. **82**, 2342 (1999).
[48] T. Paiva, G. Esirgen, R.T. Scalettar, C. Huscroft, and A. K. McMahan, e-print, cond-mat/0109497.
[49] M. E. Manley, B. Fultz, T. Swan-Wood, O. Delaire, R. J. McQueeny, E. A. Goremychkin, J. C. Cooley, W. L. Hults, J. C. Lashley, R. Osborn, and J. L. Smith (unpublished).
[50] We cite $\Delta\tau U/2$ values for $U_f = 5.81$ eV at $V = 30$ Å^3, while U_f is 4.92 and 6.27 eV at $V = 15$ and 45 Å^3, respectively.
[51] A. P. Murani, Z. A. Bowden, A. D. Taylor, R. Osborn, and W. G. Marshall, Phys. Rev. B **48**, 13981 (1993).
[52] D. M. Wieliczka, C. G. Olson, and D. W. Lynch, Phys. Rev. B **29**, 3028 (1984).
[53] E. Wuilloud, H. R. Moser, W. D. Schneider, and Y. Baer, Phys. Rev. B **28**, 7354 (1983).
[54] The f-electron Coulomb interactions have been obtained by a constrained LDA calculation and the experimental resolution has been taken from Ref. 32.
[55] These vaues are averages of n_f from Eq. (4) and $n_f^{\rm QMC} = 14[1+G(\tau=0^+)]$ from the QMC.
[56] O. Gunnarsson and K. Schönhammer, Phys. Rev. Lett. **50**, 604 (1983); Phys. Rev. B **28**, 4315 (1983); Phys. Rev. B **31**, 4815 (1983).
[57] The intuitive idea is captured by the Heitler-London ($d = 0$), $[\phi_a(1)\phi_b(2) + \phi_b(1)\phi_a(2)]/\sqrt{2}$, versus molecular orbital ($d = 1/4$), $[\phi_a(1) + \phi_b(1)][\phi_a(2) + \phi_b(2)]/2$, spatial wavefunctions for the hydrogen molecule (sites a and b). These represent completely correlated (localized) and completely uncorrelated (itinerant) ground states, respectively. The per site d values agree with the general expressions for $d_{\rm min}$ and $d_{\rm max}$ in the text, noting that the coefficient of n_f^2 in the latter is $(2z-1)/(4z)$ for z "f" orbitals per site, and $z = n_f = 1$ for the hydrogen example.
[58] N. F. Mott, Rev. Mod. Phys. **40**, 677 (1968); *Metal-Insulator Transitions* (Taylor & Francis, London, 1990).
[59] F. Gebhard, *The Mott Metal-Insulator Transition* (Springer, Berlin, 1997).